QUANTUM PHASE TRANSITIONS AND TOPOLOGICAL ORDERS IN SPIN CHAINS AND LADDERS

by

TOPLAL PANDEY

A thesis submitted in partial fulfillment

of the requirements for the degree of

Master of Science (MSc) in Physics

The School of Graduate Studies

Laurentian University

Sudbury, Ontario, Canada

THESIS DEFENCE COMMITTEE/COMITÉ DE SOUTENANCE DE THÈSE

Laurentian Université/Université Laurentienne
School of Graduate Studies/École des études supérieures

Title of Thesis Titre de la thèse	QUANTUM PHASE TRANSITIONS AND TOPOLOGICAL ORDERS IN SPIN CHAINS AND LADDERS
Name of Candidate Nom du candidat	Pandey, Toplal
Degree Diplôme	Master of Science
Department/Program Département/Programme	Physics
Date of Defence Date de la soutenance	January 27, 2014

APPROVED/APPROUVÉ

Thesis Examiners/Examinateurs de thèse:

Dr. Gennady Chitov
(Co-supervisor/Co-directeur de thèse)

Dr. Ralf Meyer
(Co-supervisor/Co-directeur de thèse)

Dr. Rizwan Haq
(Committee member/Membre du comité)

Dr. Kirill Samokhin
(External Examiner/Examinateur externe)

Approved for the School of Graduate Studies
Approuvé pour l'École des études supérieures
Dr. David Lesbarrères
M. David Lesbarrères
Director, School of Graduate Studies
Directeur, École des études supérieures

ACCESSIBILITY CLAUSE AND PERMISSION TO USE

I, **Toplal Pandey**, hereby grant to Laurentian University and/or its agents the non-exclusive license to archive and make accessible my thesis, dissertation, or project report in whole or in part in all forms of media, now or for the duration of my copyright ownership. I retain all other ownership rights to the copyright of the thesis, dissertation or project report. I also reserve the right to use in future works (such as articles or books) all or part of this thesis, dissertation, or project report. I further agree that permission for copying of this thesis in any manner, in whole or in part, for scholarly purposes may be granted by the professor or professors who supervised my thesis work or, in their absence, by the Head of the Department in which my thesis work was done. It is understood that any copying or publication or use of this thesis or parts thereof for financial gain shall not be allowed without my written permission. It is also understood that this copy is being made available in this form by the authority of the copyright owner solely for the purpose of private study and research and may not be copied or reproduced except as permitted by the copyright laws without written authority from the copyright owner.

Abstract

Dimerized antiferromagnetic spin-1/2 chains and ladders demonstrate quantum critical phase transition, the existence or absence of which is dependent on the dimerization and the dimerization pattern of the chain and the ladder, respectively. The gapped phases can not be distinguished by the conventional Landau long-range order parameters. However, they possess non-local topological string order parameters which can be used to classify different phases. We utilize the self-consistent free fermionic approximation and some standard results for exactly solved models to analytically calculate the string order parameters of dimerized spin chains. As a complement parameter the gapped phases possess the topological number, called the winding number and they are characterized by different integer values of the winding number. In order to calculate the string order parameters and winding numbers in dimerized spin chains and two-leg ladders we use analytical methods such as the Jordan-Wigner transformation, mean-field approximation, duality transformations, and some standard results available for the exactly 1D solve models. It is shown that the winding number provides the complementary framework to the string order parameter to characterize the topological gapped phases.

Acknowledgements

Formost, I would like to express my deepest and most sincere gratitute to my respected supervisors Dr. Gennady Chitov and Dr. Ralf Meyer for their motivation, continuous guidance, encouragement, and sharing the valuable time throughout the research work. It is also my pleasure to acknowledge their persistent help by supplying information, references, and the financial support, without which the work could not have been finished.

Beside my advisors, I would like to thank my other thesis committee member Dr. R. U. Haq for his valuable suggestions, comments and questions, which have definitely improved my knowledge and quality of work. Special thanks go to the Dr. Kirill Samokhin for agreeing to be my external examiner. I also wish to thank my colleague Curtis Laamanen for technical help with using computers and writing the English language, and staff of the Department of Physics for their sincere cooperation during the research work.

Last but not the least, I am deeply grateful to my parents, family members, friends, and relatives for their encouragement and support. Very special thanks go to my spouse, who sacrificed her time and companionship while this work was being completed.

Table of Contents

List of Figures

Chapter 1

Introduction

The theoretical interest in the field of low-dimensional quantum spin systems has emerged as a central area of research in condensed matter for more than a decade. The rigourous findings and investigations have proved that it is an active field in the theory of quantum materials. Most of their understood properties have been investigated by using analytical methods such as bosonization [1] and mean field approach [2] for the studies of different spin models, and also by various numerical techniques [3, 4, 5, 6, 7]. The initial review of these systems can be found in [8, 9].

The main purpose of this study is to understand the issues of the phase transitions in low-dimensional quantum spin systems and investigate hidden topological orders in the gapped phases in the dimerized spin chains and Heisenberg ladders with antiferromagnetic couplings. This chapter starts with the brief introduction of low dimensional quantum spin systems and main quantities that are calculated in the thesis.

1.1 Background

1.1.1 Spin Algebra

The intrinsic angular momentum of the fermionic electron is identified by the spin quantum number $s = 1/2$. In some solid materials the atoms acquire a total magnetic moment from the configuration of the electrons but this is not possible in many strongly correlated systems. However, the collective behaviour of such a many-particle system with strong correlations can be understood by neglecting the other electronic degrees of freedom and thinking in the terms of the physics of the localized magnetic moments [10].

The spin operators S_l^x, S_l^y and S_l^z can be readily shown to satisfy the commutation relations [11] (with $\hbar = 1$)

$$\left[S_l^\alpha, S_m^\beta\right] = i\delta_{lm}\epsilon_{\alpha\beta\gamma}S_l^\gamma \tag{1.1a}$$

and the anti-commutation relations,

$$\left\{S_l^\alpha, S_m^\beta\right\} = \frac{1}{2}\delta_{lm}\delta_{\alpha\beta} \tag{1.1b}$$

where $\epsilon_{\alpha\beta\gamma}$ is the total antisymmetric Levi-Civita tensor. The spin operators on different sites commute and on the same site anti-commute. In the spin-1/2 physics there are two state vectors given by 2 possible states of the particle. They are generally called "spin-up" and "spin-down", and written as "spin-up"$=|\uparrow\rangle = \begin{pmatrix} 1 \\ 0 \end{pmatrix}$ and "spin-down"$=|\downarrow\rangle = \begin{pmatrix} 0 \\ 1 \end{pmatrix}$. The components of the single particle spin operators

are defined in terms of Pauli matrices. They are; $S_i^\alpha = \frac{1}{2}\sigma_i^\alpha$ with $\alpha = x, y, z$ and

$$\sigma_1 = \begin{pmatrix} 0 & 1 \\ 1 & 0 \end{pmatrix}, \quad \sigma_2 = \begin{pmatrix} 0 & -i \\ i & 0 \end{pmatrix}, \quad \text{and} \quad \sigma_3 = \begin{pmatrix} 1 & 0 \\ 0 & -1 \end{pmatrix} \tag{1.2}$$

are Pauli matrices. Again, in the N particle system the components of the total spin operator S are the sum of single particle spin operators. i.e., $S^\alpha = \sum_{i=1}^{N} S_i^\alpha$.

Now we consider a two particle system with each of two spins ($\uparrow$ and $\downarrow$). There are 4 possible states found as the tensor product of 2 and 2 independent states of two particles;

$$(|\uparrow\rangle, |\downarrow\rangle) \otimes (|\uparrow\rangle, |\downarrow\rangle) = |\uparrow\rangle \otimes |\uparrow\rangle; |\uparrow\rangle \otimes |\downarrow\rangle; |\downarrow\rangle \otimes |\uparrow\rangle; |\downarrow\rangle \otimes |\downarrow\rangle \tag{1.3}$$

Thus we find the 4-dimensional state space of the two particle system. Therefore by extension of this reasoning we can see that the dimension of the N-particle spin space for spin-1/2 is 2^N. To represent the 4- dimensional state space, gamma matrices are constructed as a tensor product of Pauli matrices [12, 13]. They are given by:

$$\Gamma_1 = \sigma_1 \otimes \mathbb{1} \qquad \Gamma_2 = \sigma_2 \otimes \mathbb{1} \qquad \Gamma_{3,4,5} = \sigma_3 \otimes \sigma_{1,2,3} \tag{1.4}$$

and satisfy the algebraic relations $\{\Gamma_a, \Gamma_b\} = 2\delta_{a,b}$ and $\Gamma_{ab} = \frac{1}{2i}[\Gamma_a, \Gamma_b]$.

1.1.2 Physical Properties of Spin Chains

It is known that the intuition which derived from the classical vision of spin is surprisingly different with the outcomes from the quantum mechanical models. In order to understand such peculiarities the spin-1/2 chain may be an example of one dimensional quantum systems. Here we provide only brief outlines of the most

important properties, further detail of the study can be found in [14]

In general, we assume the localized spins interact via nearest neighbour exchange, called exchange interaction. Rather it arises as a result of the Pauli exclusion principle for the indistinguishable particles. For fermions, it demands that the total wavefunction $\Phi(r_1, r_2, \sigma_1, \sigma_2) = \phi(r_1, r_2)\psi(\sigma_1, \sigma_2)$ must be antisymmetric under the simultaneous exchange of both space wavefunction $\phi(r_1, r_2)$ and spin wavefunction $\psi(\sigma_1, \sigma_2)$ of the particles [15]. Thus the symmetric and anti-symmetric spin wavefunctions provided different energy levels so that the difference in energy is added into the interaction energy.

The Hamiltonian that provides the information of spin-spin interaction is the spin Hamiltonian. It is also popularly known as Heisenberg Hamiltonian and it is given by

$$H = \sum_{ij} J_{ij}\ \mathbf{S}_i \mathbf{S}_j \tag{1.5}$$

where J_{ij} are known as exchange coupling constants and S_i denotes total spin operators at site i. In the standard Heisenberg Hamiltonian only nearest neighbour interaction is taken into account. Thus $J_{ij} = J =$ constant. If $J > 0$, the models favors antiferromagnetic orderings with the antiparallel alignment of spins. If $J < 0$, the model favors ferromagnetic orderings with all spins aligned along the same axis. The Heisenberg spin chain can be taken as an example of a spin system to discuss spin algebra. The Hamiltonian of the system for the nearest neighbour interaction between the sites i and $i + 1$ is expressed as

$$H = \sum_{i=1}^{N} \left[J_{xy} \left(S_i^x S_{i+1}^x + S_i^y S_{i+1}^y \right) + J_z S_i^z S_{i+1}^z \right] \tag{1.6}$$

where N is the number of sites in the chain. In the isotropic chain with uniform

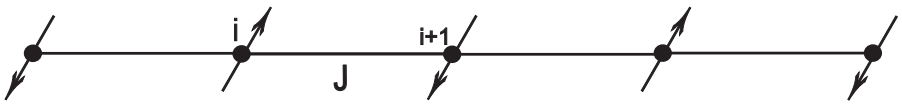

Figure 1.1: Heisenberg spin chain. The arrows represent spins at each site i and the solid line represents the exchange coupling J.

antiferromagnetic couplings $J_{xy} = J_z$ then long range order is prevented due to the strong quantum fluctuations [16]. This spin chain is illustrated in Fig. 1.1. When $J_z = 0$ the model becomes the XY model and it is exactly solvable using the Jordan-Wigner transformation [17] . The details on such transformation are given in chapter 2.

For analysing the Hamiltonian of spin models it is convenient to use the raising and lowering spin operators, defined as follows:

$$S_i^{\pm} = S_i^x \pm iS_i^y \tag{1.7}$$

which obey the following canonical anti-commutation relations;

$$\left\{S_i^-, S_j^+\right\} = \delta_{ij} \tag{1.8a}$$

$$\left\{S_i^-, S_j^-\right\} = \left\{S_i^+, S_j^+\right\} = 0 \tag{1.8b}$$

For the uniform spin- 1/2 chain with even number of spins it is known that the ground state has zero spin (singlet state) [18], i.e, $\langle S\rangle = 0$. This non-degenerate state exhibits gapless excitations, which means no energy is required to excite the spin. The other important spin system is the gapped spin system where the gap is said to be the difference between the energies of lowest excited state and the ground

state. Thus, the gap energy (Δ) is the minimum energy required to excite the spin from the ground state to first excited state.

The dimerized spin system may be one example of a gapped system in which dimerizarization refers to the modulation of the exchange coupling J along the chain by the parameter δ. Here δ is the dimerization parameter in the range between 0 and 1. Thus the coupling of a Heisenberg chain with dimerization has stronger and weaker bonds alternation with

$$J \to J(1 + (-1)^i \delta) \tag{1.9}$$

where i is the number of the site. Such a Heisenberg model is illustrated in Fig. 1.2. The dimerized Heisenberg model is technically very difficult and there are still

Figure 1.2: The dimerized spin chain. The arrows represent the spin at each lattice site, and thick and thin lines represent the modulated exchange couplings $J(1+\delta)$ and $J(1-\delta)$, respectively.

some problems left on the way of a exact solution. So, we illustrate the important results by taking the XY-limit [14]. This model allows us to map the spin system onto free spinless fermions such that the free energy is

$$f(T,\delta) = \frac{F}{N} = -\frac{\ln 2}{\beta} - \frac{2}{\pi\beta}\int_0^{\frac{\pi}{2}} \ln\cosh\left(\frac{\beta}{2}\epsilon(k)\right) dk \tag{1.10}$$

with the spectrum [19, 20]

$$\epsilon(k)^{\pm} = \pm J\sqrt{\cos^2 k + \delta^2 \sin^2 k} \tag{1.11}$$

By looking at Eq. (1.11), we realize that the XY model has the gap in its spectrum, and the gap $\Delta = J\delta$ has linear dependence on the dimerization.

1.1.3 Haldane Conjecture

In 1983, Haldane conjectured that the ground state of the spin-1 and spin-1/2 anti-ferromagnetic Heisenberg spin chains were fundamentally different. He conjectured that the spin-1 system is gapped whereas spin-1/2 system shows the gapless behaviour [21]. This conjecture has been widely accepted in the research field even though the rigorous proof has not been found yet. It is, however, supported by the large number of theoretical and numerical works.

1.1.4 Physical Properties of Spin Ladders

Spin ladders are low dimensional systems in which inter-chain coupling is taken into account in addition to the intra-chain coupling J on the finite number of interacting spin chains. This coupling is also called rung coupling and will be denoted by $J_\perp$. Thus, the additional interaction rung term can be represented in the form of Hamiltonian as below:

$$H_{rung} = J_\perp \sum_{\alpha,\beta,i} S_{i,\alpha} S_{j,\beta} \tag{1.12}$$

where α and β are chain indices, and i is the site index. Hence, the Hamiltonian of spin-1/2 anti-ferromagnetic Heisenberg m-leg ladder is expressed as follows:

$$H = \sum_{i=1}^{N} \left[J \sum_{\alpha=1}^{m} S_\alpha(i) S_\alpha(i+1) + J_\perp \sum_{\alpha=1}^{m-1} S_\alpha(i) S_{\alpha+1}(i) \right] \tag{1.13}$$

with total number of spins $N \times m$. Here α and i are the chain and site indices, respectively. A two-leg spin ladder is shown in Fig. 1.3.

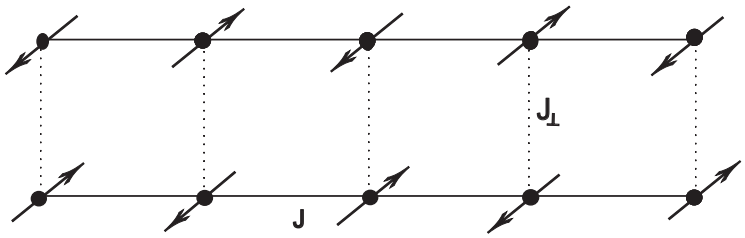

Figure 1.3: A two-leg spin ladder. The arrows represent spins at each sites of ladder, solid and dashed lines represent the intra-chain coupling J and inter-chain coupling $J_\perp$, respectively.

One of the most important properties of the spin ladder is the existence or absence of spin gap, and it depends only on the number of legs in the ladder. The spin excitations are gapped for the even-legged ladders and gapless for odd-legged ladders [8, 22]. To understand such a peculiar property of ground state of spin-1/2 ladder, we take a two-leg ladder in the strong rung coupling limit, i.e., $J_\perp \gg J$. Then the spins are locked in rung by forming the group of singlets. From the spectrum of two spin $J\overrightarrow{S_1}\overrightarrow{S_2}$ their lowest energy singlet state is separated from the triple state by the energy gap J. Hence, a finite energy (gap) is needed in the two-leg ladder to break the rung singlet. In addition, new featuring physics appears when legs in the ladder are dimerized. The properties of dimerized two-leg ladder are quite different in the different dimerization patterns. In chapter 3 we will discuss the details of such spin system by determining the quantities such as ground state energy, energy spectrum, energy gap, etc.

On the other hand, the three leg spin-1/2 ladder can be reduced to the single spin-1/2 chain, which is always gapless [14]. This odd/even alternation between gapped and gapless ladders is highly reminiscent of Haldane conjecture for the half integer and integer spin chains. The even legged spin-1/2 ladder with strong rung coupling is represented as equivalent to the spin-1 chain [23].

1.2 Quantum Phase Transitions

1.2.1 Symmetry Breaking and Order Parameters

A general example of phase transitions is the change of states (solid, liquid and gas) of matter. In such transitions latent heat plays a vital role to modify the crystalline structure. In terms of crystal modifications, the crystal lattice suddenly rearranges and converts into another state of matter. These are called first order phase transitions. In a phase transition the symmetry that characterises the phase of one state, is not present in the other phase. For example: fluid-solid phase transition. In such transitions the fluids are said to have continuous translational symmetries and they are broken into discrete translational symmetries in crystalline solids.

Next example of the symmetry breaking at the transition point is the ferromagnetic transition. At high temperature the thermal fluctuations keep ordered magnetic domains from forming resulting in zero magnetisation. If the temperature is lowered below the Curie temperature T_c, the magnetic moments within the domains start to align and a non-zero magnetisation appears. Here, the low-temperature ferromagnetic phase spontaneously breaks the spin-inversion symmetry. This type of transition of symmetry-breaking is called second order phase transition or thermal phase transition. These previously mentioned two examples of phase transitions are also called classical phase transitions.

The famous and commonly focused phase transitions are quantum phase transitions. These transitions occur between two quantum phases at zero temperature due to the change of some parameters. Interestingly, the quantum systems have fluctuations driven by the Heisenberg uncertainty principle even in the ground state

[24]. The quantum Ising model can be taken as a suitable example to understand such a phase transition. The Hamiltonian of the Ising spin chain in a transverse magnetic field is given by

$$H = J \sum_{\langle i,j \rangle} S_i^z S_j^z + h \sum_i S_i^x \tag{1.14}$$

where J is the exchange coupling of nearest neighbour $\langle i, j \rangle$ spin interaction and h is the external transverse magnetic field. By looking at Eq. (1.14) it is seen that the ground state of the system can only depend on the ratio of parameters J/h. In the limit $J/h \gg 1$ the first term of Eq. (1.14) dominates and the ground state is magnetically ordered. Thus the magnetisation $\langle S^z \rangle$ appears in this limit. It is an example of the order parameter. Next, we consider the opposite limit $J/h \ll 1$ then we find that the ground state is qualitatively different. At this limit the second term of Eq. (1.14) dominates by resulting in a non-zero magnetisation $\langle S^x \rangle$ for the system. Here we find the energy gap $\Delta \sim |J - h|$ from the spectrum calculated in [24, 25]. Thus the spin system is critical at $J = h$ and gapped otherwise. The different gapped phases on either side of the critical point $J = h$ are characterized by the order parameter. It gives the measure of the ferromagnetic order present in each phase. An order parameter of the quantum system is zero in the disordered phase and grows continuously to its maximum value in its ordered phase.

1.2.2 Landau's Theory of Second Order Phase Transitions

In his history of *second order phase transitions* Landau postulated that the symmetry of one phase is always higher than the other phase but that the symmetries of the two phases are entirely unrelated in *first order phase transitions*. It is the most widely used formalism to describe such phase transitions. Phase transitions are

characterized by the singularity of thermodynamical quantities such as thermodynamic potential Φ. The order parameter grows continuously from zero at transition point and it is small and uniform near the transition point. According to Landau the thermodynamic potential near the transition point can be expressed as an expansion over the order parameter [26]. It is given by

$$\Phi(P, T, \eta) = \Phi_0 + A\eta + B\eta^2 + C\eta^3 + D\eta^4 + ... \tag{1.15}$$

where $A, B, C, D....$ are functions of pressure and temperature, and couplings at zero temperature. η is the order parameter near the transition point. Thus the thermodynamic potential must obey all possible symmetries of the order parameter.

The thermal ferromagnetic transition in the Ising model introduced in the section 1.2.1 is a suitable example . The system satisfies the spin-inversiton symmetry in terms of magnetisation M as an order parameter. This means the free energy f must be invariant under $M \to -M$, i.e., only even powers are permitted in the expansion of f. The free energy [27] is

$$f(T, M) = \Phi_0 + \frac{1}{2}a(T - T_c)M^2 + \frac{1}{4}cM^4 + ... \tag{1.16}$$

The stable states of the system are found by minimising the free energy. They are:

$$M = \begin{cases} 0 & T > T_c \\ \pm\sqrt{\frac{a(T-T_c)}{c}} & T < T_c \end{cases} \tag{1.17}$$

The expression for the free energy gives two solutions for the nontrivial order parameter and the system will spontaneously choose only one, that's why spontaneously breaking the symmetry.

1.2.3 Critical Point Exponents

It is very important to know the behaviour of the spin system near the transition point of the *second order phase transition*. The transition point is also called the critical point and the behaviour of system at the critical point is called criticality. The critical behaviour can be classified in terms of critical exponents. In thermal phase transition the theory of critical exponents has been reviewed in [26, 28]. It is also reviewed by Sachdev [24] in the case of quantum criticality.

We consider the function $f(\epsilon)$ of quantum system with coupling g where

$$\epsilon = \frac{g - g_c}{g} \tag{1.18}$$

is a dimensionless variable which measures the distance from the critical point g_c. The system parameters such as magnetisation $M(\epsilon)$ and correlation length ξ can be expressed in the same way. If the function is positive and continuous then we can write the parameter

$$\lambda = \lim_{\epsilon \to 0} \frac{\ln f(\epsilon)}{\ln \epsilon} \tag{1.19}$$

called the critical exponent. The notation of critical exponents of specific quantities has been standardized. For example the critical exponents of correlation length ξ is ν with the relation

$$\xi \propto \mid g - g_c \mid^{-\nu} \tag{1.20}$$

In addition the critical exponents of the order parameter, specific heat, and susceptibility are β, α, and γ respectively. Here they are related via the scaling relations [27]

$$\alpha + 2\beta + \gamma = 2 \tag{1.21a}$$

$$\gamma + 2\beta = d\nu \tag{1.21b}$$

$$\alpha + d\nu = 2 \tag{1.21c}$$

where d is the system's dimension. In case of short-ranged interactions the value of critical exponent is determined by the number of components (dimension) of the system. Therefore different systems can be categorized by the values of critical exponents. This phenomenon is called universality [27]

1.3 Spin Duality Transformation

We define a one dimensional dual lattice of a system as a new lattice with its sites located at the mid-points of the old lattice. Fig. 1.4 shows the dual and the original lattices. Here we consider the σ and τ operators defined on the sites of the original

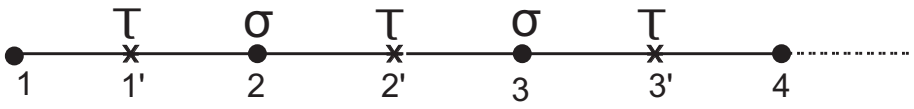

Figure 1.4: Real and dual lattice in 1D system adapted from Reference [29].

and dual lattice, respectively. Both operators σ and τ obey the Pauli spin algebra

$$\left[\sigma_i^\alpha, \sigma_j^\beta\right] = 2i\delta_{ij}\epsilon_{\alpha\beta\gamma}S_i^\gamma \tag{1.22a}$$

and the anti-commutation relations,

$$\left\{\sigma_i^\alpha, \sigma_j^\beta\right\} = \frac{1}{8}\delta_{ij}. \tag{1.22b}$$

They are related by the following dual transformations [29].

$$\sigma_j^x = \tau_{j-1}^x \tau_j^x \tag{1.23a}$$

$$\sigma_j^y = \prod_{k=j}^{N} \tau_k^y \tag{1.23b}$$

This transformation $\sigma \to \tau$ is called the spin duality transformation. The operators σ_i^α and τ_i^α with $\alpha = x, y, z$; are 2×2 Pauli spin matrices and N is the total number of sites in the chain. By using the above relations and the Pauli matrix the operators on the original lattice can be mapped onto the dual lattice operators and vice versa. To verify the commutation relations in the dual space, let us take Eqs. (1.23a) and (1.23b) and plug $\sigma \to S$ in terms of $\tau \to S$ in Eq. (1.1b) to obtain

$$\tau_{j-1}^x \tau_j^x \prod_{k=j}^{N} \tau_k^y = -\tau_j^y \left(\prod_{k=j+1}^{N} \tau_k^y \right) \tau_{j-1}^x \tau_j^x \tag{1.24}$$

where we have used the relation $S_i^\alpha = (1/2)\sigma_i^\alpha$. We use again the duality transformation (1.23a) and (1.23b) in the commutation relation (1.1a) and then plug it into Eq. (1.24). This yields

$$\tau_{j-1}^x \tau_j^x \tau_j^y = -\tau_j^y \tau_{j-1}^x \tau_j^x \tag{1.25}$$

From Eq. (1.25) we come to the following conclusion:

$$\{\tau_j^x, \tau_j^y\} = 0 \tag{1.26a}$$

if and only if,

$$\left[\tau_{j-1}^x, \tau_j^y\right] = 0 \tag{1.26b}$$

Eqs. (1.26a) and (1.26b) are anti-commutation and commutation relations, respectively and they are satisfied by the τ operator in the dual lattice. Thus the mapping of the operators on the direct lattice onto the operators on the dual lattice preserves the correct anti-commutation relations.

1.4 String Order Parameter (SOP)

The dimerized spin-1/2 systems, i.e., dimerized chains and ladders are special quantum systems in which gap (mass) formation is not attributed to some local symmetry breaking. This seems to go against the postulate of the Landau Theory. We define uniquely new orders which have no physical relations with the direct system but it can be related to hidden symmetries in the system under transformation. Such hidden order parameter is called the string order parameter. We will use the string order parameters to distinguish the different gapped phases in the dimerized spin models.

1.4.1 String Order Parameter in the Spin Chain

den Nijs and Rommelse [30] introduced string order parameters in the spin-1 antiferromagnetic system and pointed out that it can be used to distinguish the gapped phase from other phases. It is known that the string order parameter gives the measure of a hidden (non-local) symmetry breaking [31] in the spin-1 chains. Such symmetries are broken in the gapped phase and unbroken in the other phases.

The string order parameter has been defined for spin systems [9] as

$$O^{\alpha} = -\lim_{|i-j|\to\infty} \left\langle S_i^{\alpha} \exp\left[i\pi \sum_{k=i+1}^{j-1} S_k^{\alpha} \right] S_j^{\alpha} \right\rangle \tag{1.27}$$

where, $\alpha = x, y, z$ and S_i^{α} is the spin operator at site i.

Let us use the relation $S_i^{\alpha} = (1/2)\sigma_i^{\alpha}$ between the spin and Pauli matrices in Eq. (1.27) and choose the cyclic boundary condition $\sigma_{N+1} \equiv \sigma_1$ in the spin chain of

N sites. Then we have,

$$O^x = -\frac{1}{4}\lim_{N\to\infty}\left\langle \sigma_1^x \exp\left[\frac{i\pi}{2}\sum_{k=2}^{N-1}\sigma_k^x\right]\sigma_N^x\right\rangle \tag{1.28}$$

The phase terms $e^{\left[\frac{i\pi}{2}\sum_{k=2}^{N-1}\sigma_k^x\right]}$ of the string order parameter can be written as a product:

$$\exp\left[\frac{i\pi}{2}\sum_{k=2}^{N-1}\sigma_k^x\right] = \prod_{k=2}^{N-1}\exp\left(\frac{i\pi}{2}\sigma_k^x\right) \tag{1.29}$$

From the well-known relation

$$\exp\left(i\theta\sigma_k^x\right) = \cos\theta + i\sigma_k^x\sin\theta \tag{1.30}$$

we have

$$\exp\left(\frac{i\pi}{2}\sigma_k^x\right) = i\sigma_k^x \tag{1.31}$$

Assuming even number of sites in the chain, i.e., $N = 2l$, the SOP (1.28) reads as

$$O^x = \frac{1}{4}\lim_{l\to\infty}(-1)^l\left\langle\prod_{k=1}^{2l}\sigma_k^x\right\rangle \tag{1.32}$$

Note that the SOP for the odd number of sites in the chain, i.e., $N = 2l+1$, always vanishes due to the symmetry.

Now we take the product of σ operators in Eq. (1.32) and apply the duality transformation (1.23a) resulting in

$$\prod_{k=1}^{2l}\sigma_k^x = \tau_0^x\tau_1^x\tau_1^x\tau_2^x.....\tau_{2l-1}^x\tau_{2l}^x = \tau_0^x\tau_{2l}^x \tag{1.33}$$

i.e., the term $\tau_0^x\tau_{2l}^x$ on the dual lattice corresponds to the string product of $2l$ oper-

ators in the original lattice. We use the relation $(\tau_l^x)^2 = 1$, for all $l = 1, 2, ...$ in the above equation.

Here, we are interested in the string order parameter. For this purpose we plug Eq. (1.33) into Eq. (1.32) to obtain

$$O^x = \frac{1}{4} \lim_{l \to \infty} (-1)^l \langle \tau_0^x \tau_{2l}^x \rangle \tag{1.34}$$

So, the non-local SOP defined on the sites of direct lattice becomes a local order parameter on the dual lattice. As we will discuss in more detail later, the above result suggests that the Landau theory of the continuous phase transition is applicable in terms of the dual operators.

1.4.2 String Order Parameters in Ladders

The generalized string order parameters of two-leg spin ladders have been defined in [32, 33, 34, 35, 36] as

$$O^z_{odd} = \lim_{|n-m| \to \infty} O^z_{odd}(|n-m|)$$

$$O^z_{odd} = -\langle (S^z_1(n) + S^z_2(n)) \exp \left[i\pi \sum_{l=n+1}^{m-1} (S^z_1(l) + S^z_2(l)) \right] (S^z_1(m) + S^z_2(m)) \rangle \tag{1.35}$$

The illustration of these two string order parameters is shown in the Fig. 1.5

where $S^z_1(n)$ and $S^z_2(n)$ are two spin-1/2 operators at the site i in the chain 1 and 2 respectively. Here, the rung chains are summed up in case of odd string parameter between the infinite limit of sites n and m. Again,the even string order parameter is defined by summing the diagonal spins of the ladder. It is given by

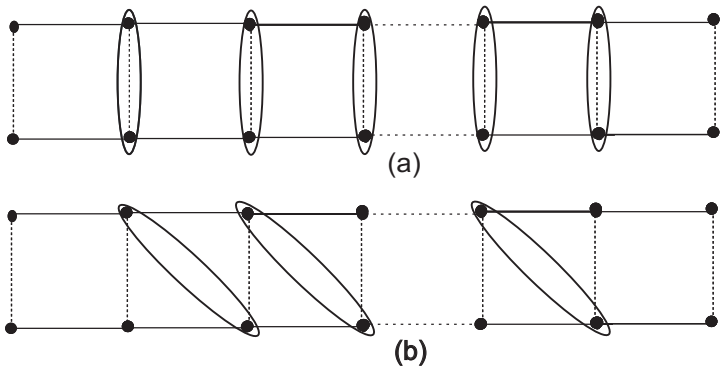

Figure 1.5: An illustration of (a) odd and (b) even string order parameters for two-leg ladder.

$$O^z_{even} = \lim_{|n-m|\to\infty} O^z_{even}(|n-m|)$$

$$= -\langle (S^z_1(n) + S^z_2(n+1)) \exp\left[i\pi \sum_{l=n+1}^{m-1} (S^z_1(l) + S^z_2(l+1)) \right] (S^z_1(m) + S^z_2(m+1)) \rangle \tag{1.36}$$

The illustration of these two string order parameters is shown in the Fig. 1.5

1.5 Winding Number

In the section 1.4. we have defined the string order parameter (SOP) to characterize the unconventional phases, called topological phases in the spin chains and ladders. Alternatively, the topological phases can be classified by defining another topological parameter called winding number or Pontryagin index. It counts the number of loops formed by the normalized vectors in the topological phases over the Brillouin zone by wrapping the phases around the centre of the energy plane. The normalized vectors and the dimension of topological phases are defined by the spectrum of the model in the momentum space. For the one dimensional case the winding number

[2, 37] is defined as

$$N_w = \frac{1}{2\pi} \oint_c \left(n_x(k) \frac{\partial n_y(k)}{\partial k} - n_y(k) \frac{\partial n_x(k)}{\partial k} \right) dk \tag{1.37}$$

where $n(k) = (n_x(k), n_y(k))$ is the normalized vector $n = \mathbf{d}/|d|$ that resides in the unit circle, and k is the wavevector in momentum space that spans over the Brillouin zone. The Hamiltonian matrix [38] written in the form of $\mathcal{H}(k) = \mathbf{d}.\sigma$. The vector function $n(k)$ well-defines the mapping everywhere from the Brillouin zone to the $(n_x(k), n_y(k))$ plane [2, 37, 39, 40] and it characterizes the topological gapped phases.

Chapter 2

Anisotropic Dimerized XY Chain

In this chapter we study the exactly solvable anisotropic dimerized XY spin-1/2 chain in the alternating transverse magnetic field. In order to solve the model and find such quantities as energy spectrum, ground state energy, and energy gap, etc. we use the Jordan-Wigner transformation (JWT). It maps the spin-1/2 operators onto the non-interacting spinless fermion operators. The advantage of using such transformation is that it always preserves the spin commutation relations based on Pauli's exclusion principle. In this chapter, we will provide a brief review of the one dimensional JWT by analysing the above mentioned model.

2.1 The Hamiltonian

We start by writing the Hamiltonian of the anisotropic dimerized XY spin-1/2 chain in an alternating transverse magnetic field. It is

$$H = J\sum_{i=1}^{N}\left[(1+\gamma)S_i^xS_{i+1}^x + (1-\gamma)S_i^yS_{i+1}^y + (-1)^i\delta\left(S_i^xS_{i+1}^x + S_i^yS_{i+1}^y\right)\right]$$

$$+\sum_{i=1}^{N}(-1)^i h S_i^z \tag{2.1}$$

where S_i^α are spin-1/2 operators with $\alpha = x, y, z$; satisfying the standard spin commutation relations (1.1a) and (1.1b). N is the number of spins, and open boundary conditions are assumed. The exchange coupling of the nearest neighbours is J. $\gamma \in [0, 1]$ is the parameter characterizing the degree of the xy anisotropy, δ is the dimerization parameter and, h is the magnitude of the alternating external magnetic field. This anisotropic dimerized XY chain in the transverse magnetic field has been proposed in [41] to study the quantum Ising criticality. To the best of our knowledge this model in the alternating transverse field has never been studied before.

To analyze the spin Hamiltonian (2.1) it is convenient to use the raising and lowering spin operators; S_i^+ and S_i^- as defined in the Eq.(1.7). These operators satisfy the commutation relations (1.8a) and (1.8b). Using Eq. (1.7) the Hamiltonian (2.1) can be written in terms of the raising and lowering spin operators as

$$H = \frac{1}{2}\sum_{i=1}^{N} J\left(1 + (-1)^i\delta\right)\left(S_i^+ S_{i+1}^- + S_i^- S_{i+1}^+\right)$$

$$+\frac{\gamma}{2}\sum_{i=1}^{N}\left[J\left(S_i^+ S_{i+1}^+ + S_i^- S_{i+1}^-\right) + (-1)^i h\left(2S_i^+ S_i^- - 1\right)\right] \tag{2.2}$$

2.1.1 Review of Jordan-Wigner Transformation (JWT)

In order to solve the model (2.2) we use the transformation due to Jordan and Wigner [17] who used it to map spin operators onto spinless fermion operators.

The JWT from spin to fermion operators is defined as

$$S_i^+ = c_i^\dagger \exp\left(i\pi \sum_{l=1}^{i-1} n_l\right) \tag{2.3a}$$

$$S_i^- = \exp\left(-i\pi \sum_{l=1}^{i-1} n_l\right) c_i \tag{2.3b}$$

$$S_i^z = c_i^\dagger c_i - \frac{1}{2} \tag{2.3c}$$

where and $c_i^\dagger$ and c_i are fermionic creation and annihilation operators, respectively. One can check that the JW fermion operators obey the canonical anti-commutation relations:

$$\{c_i, c_j^\dagger\} = \delta_{ij} \qquad \{c_i, c_j\} = 0 \qquad \{c_i^\dagger, c_j^\dagger\} = 0 \tag{2.4}$$

In the above equations $n_i = c_i^\dagger c_i$ is the occupation number operator satisfying the well-known relation

$$n_i = n_i^2 \tag{2.5}$$

In order to demonstrate how the JWT preserves the spin commutation relations, we take the phase term at ith lattice site and expand it as

$$\begin{aligned} e^{i\pi n_i} &= 1 + (i\pi)n_i + \frac{1}{2!}(i\pi)^2 n_i^2 + \frac{1}{3!}(i\pi)^3 n_i^3 + ... \\ &= 1 + n_i(1 + i\pi + \frac{1}{2!}(i\pi)^2 + \frac{1}{3!}(i\pi)^3 + ... - 1) \\ &= 1 + n_i(e^{i\pi} - 1) = 1 - 2n_i = 1 - 2c_i^\dagger c_i \end{aligned} \tag{2.6}$$

where the relation (2.5) has been used in the second line of Eq. (2.6).

To understand the role of the phase term in the JWT, Eq. (2.6) is multiplied

by the operator $c_i^\dagger$ from the left. The result is

$$c_i^\dagger e^{i\pi n_i} = c_i^\dagger(1 - 2c_i^\dagger c_i) = c_i^\dagger - 2c_i^\dagger c_i^\dagger c_i = c_i^\dagger \tag{2.7}$$

where the Pauli exclusion principle condition $(c_i^\dagger)^2 = 0$ is used. Multiplying Eq. (2.6) by the operator $c_i^\dagger$ from right, we get

$$e^{i\pi n_i} c_i^\dagger = (1 - 2c_i^\dagger c_i)c_i^\dagger = c_i^\dagger - 2c_i^\dagger c_i c_i^\dagger$$

$$= c_i^\dagger - 2c_i^\dagger(1 - c_i^\dagger c_i) = -c_i^\dagger + 2c_i^\dagger c_i^\dagger c_i = -c_i^\dagger \tag{2.8}$$

The anti commutation relation (2.4) has been used in the second line of Eq. (2.8). Similarly, by multiplying Eq. (2.6) by the operator c_i from the left and right, and applying anti commutation relations (2.4), we derive

$$c_i e^{i\pi n_i} = -c_i \tag{2.9a}$$

$$e^{i\pi n_i} c_i = c_i \tag{2.9b}$$

So we can write the following proporties of the fermionic operator at the same site

$$c_i^\dagger e^{i\pi n_i} = -e^{i\pi n_i} c_i^\dagger, \quad \text{and} \quad c_i e^{i\pi n_i} = -e^{i\pi n_i} c_i \tag{2.10}$$

Similarly for the different sites the fermionic operators satisfy

$$c_i^\dagger e^{i\pi n_j} = e^{i\pi n_j} c_i^\dagger, \quad \text{and} \quad c_i e^{i\pi n_j} = e^{i\pi n_j} c_i \quad \text{for} \quad i \neq j \tag{2.11}$$

To check the spin commutation relations at the same site we have

$$\left[S_i^+, S_i^-\right] = S_i^+ S_i^- - S_i^- S_i^+$$

$$= \exp\left(-i\pi \sum_{k=1}^{i-1} n_k\right) c_i^\dagger c_i \exp\left(i\pi \sum_{k=1}^{i-1} n_k\right) - c_i \exp\left(i\pi \sum_{k=1}^{i-1} n_k\right) \exp\left(-i\pi \sum_{k=1}^{i-1} n_k\right) c_i^\dagger$$

$$= c_i^\dagger c_i - c_i c_i^\dagger = c_i^\dagger c_i - (1 - c_i^\dagger c_i) = 2c_i^\dagger c_i - 1 = 2S_i^z \tag{2.12}$$

Thus we find the correct commutation relations. Similarly, we check that

$$\left[S_i^-, S_i^-\right] = \left[S_i^+, S_i^+\right] = 0 \tag{2.13}$$

For different sites we take $j > i$ and find

$$\left[S_i^-, S_j^-\right] = S_i^- S_j^- - S_j^- S_i^-$$

$$= c_i \exp\left(i\pi \sum_{k=1}^{i-1} n_k\right) c_j \exp\left(i\pi \sum_{k=1}^{j-1} n_k\right) - c_j \exp\left(i\pi \sum_{k=1}^{j-1} n_k\right) c_i \exp\left(i\pi \sum_{k=1}^{i-1} n_k\right)$$

$$= (c_i c_j + c_j c_i) \exp\left[i\pi \left(\sum_{k=1}^{i-1} n_k + \sum_{k=1}^{j-1} n_k\right)\right] = 0 \tag{2.14}$$

where we used $e^{i\pi n_i} c_i = -c_i e^{i\pi n_i}$ in the second line and $\{c_i, c_j\} = 0$ in the third line of Eq. (2.14). Finally from the Eqs. (2.12), (2.13) and (2.14) it is seen that the spin commutation relations are preserved by the JWT. The key role of the phase factor in JWT is clear from the above derivations.

So each spin raising and lowering operator in the Hamiltonian (2.2) can be mapped onto the fermion operator by using the JWT. We rewrite the following

terms

$$S_i^+ S_{i+1}^- = \exp\left(-i\pi \sum_{k=1}^{i-1} n_k\right) c_i^\dagger c_{i+1} \exp\left(i\pi \sum_{k=1}^{i} n_k\right)$$

$$= c_i^\dagger e^{i\pi n_i} c_{i+1} = c_i^\dagger c_{i+1}, \tag{2.15a}$$

$$S_i^- S_{i+1}^+ = c_i \exp\left(i\pi \sum_{k=1}^{i-1} n_k\right) \exp\left(-i\pi \sum_{k=1}^{i} n_k\right) c_{i+1}^\dagger$$

$$= c_i e^{-i\pi n_i} c_{i+1}^\dagger = -c_i c_{i+1}^\dagger = c_{i+1}^\dagger c_i, \tag{2.15b}$$

$$S_i^+ S_{i+1}^+ = \exp\left(-i\pi \sum_{k=1}^{i-1} n_k\right) c_i^\dagger \exp\left(-i\pi \sum_{k=1}^{i} n_k\right) c_{i+1}^\dagger$$

$$= c_i^\dagger \exp\left(-2i\pi \sum_{k=1}^{i-1} n_k\right) e^{-i\pi n_i} c_{i+1}^\dagger = c_i^\dagger c_{i+1}^\dagger, \text{ with } e^{\pm 2i\pi n_i} = 1 \tag{2.15c}$$

$$S_i^- S_{i+1}^- = c_i \exp\left(i\pi \sum_{k=1}^{i-1} n_k\right) c_{i+1} \exp\left(i\pi \sum_{k=1}^{i} n_k\right)$$

$$= c_i \exp\left(2i\pi \sum_{k=1}^{i-1} n_k\right) e^{i\pi n_i} c_{i+1} = -c_i c_{i+1} = c_{i+1} c_i, \tag{2.15d}$$

and

$$S_i^+ S_i^- = \exp\left(-i\pi \sum_{k=1}^{i-1} n_k\right) c_i^\dagger c_i \exp\left(i\pi \sum_{k=1}^{i-1} n_k\right) = c_i^\dagger c_i \tag{2.15e}$$

Then the Hamiltonian (2.2) becomes

$$H = \frac{J}{2} \sum_{i=1}^{N} \left(1 + (-1)^i \delta\right) \left(c_i^\dagger c_{i+1} + c_{i+1}^\dagger c_i\right)$$

$$+ \frac{\gamma}{2} \sum_{i=1}^{N} \left[J\left(c_i^\dagger c_{i+1}^\dagger + c_{i+1} c_i\right) + (-1)^i h \left(2 c_i^\dagger c_i - 1\right)\right] \tag{2.16}$$

2.1.2 Fourier Transformation

To simplify further the quadratic Hamiltonian (2.16), the chain is divided into even and odd sites. The resulting Hamiltonian is in the following form:

$$H = \frac{1}{2}\sum_{i=1}^{N/2}\left[J(1+\delta)\left(c_{2i}^{\dagger}c_{2i+1} + c_{2i+1}^{\dagger}c_{2i}\right) + J\gamma\left(c_{2i}^{\dagger}c_{2i+1}^{\dagger} + c_{2i+1}c_{2i}\right) + 2hc_{2i}^{\dagger}c_{2i}\right]$$

$$+\frac{1}{2}\sum_{i=1}^{N/2} J(1-\delta)\left(c_{2i+1}^{\dagger}c_{2i+2} + c_{2i+2}^{\dagger}c_{2i+1}\right) + J\gamma\left(c_{2i+1}^{\dagger}c_{2i+2}^{\dagger} + c_{2i+2}c_{2i+1}\right)$$

$$-h\sum_{i=1}^{N/2} c_{2i+1}^{\dagger}c_{2i+1} \tag{2.17}$$

We introduce the Fourier transforms of the fermion operators at odd and even sites, as follows:

$$c_{2n} = \sqrt{\frac{2}{N}}\sum_{k} e^{-i2nk}d_e(k) \tag{2.18a}$$

and

$$c_{2n+1} = \sqrt{\frac{2}{N}}\sum_{k} e^{-ik(2n+1)}d_o(k) \tag{2.18b}$$

where $d_{o,e}(k)$ are Fourier transforms of fermi operators on the odd and even sites, respectively. k is the wavevector in the momentum space within the first Brillouin zone $[\frac{-\pi}{2}, \frac{\pi}{2}]$. Now we can rewrite the terms of the Hamiltonian (2.1.2) in the momentum space:

$$\sum_{i=1}^{N/2} c_{2i}^{\dagger}c_{2i+1} = \sum_{i=1}^{N/2}\sqrt{\frac{2}{N}}\sum_{k} e^{ik(2i)}d_e(k)\sqrt{\frac{2}{N}}\sum_{k} e^{-ik(2i+1)}d_o(k)$$

$$= \sum_{k} e^{-ik}d_e^{\dagger}(k)d_o(k) = \sum_{k>0}\left(e^{-ik}d_e^{\dagger}(k)d_o(k) + e^{ik}d_e^{\dagger}(-k)d_o(-k)\right) \tag{2.19a}$$

and

$$\sum_{i=1}^{N/2} c_{2i}^{\dagger} c_{2i+1}^{\dagger} = \sum_{k>0} \left(e^{-ik} d_e^{\dagger}(k) d_o^{\dagger}(-k) + e^{ik} d_e^{\dagger}(-k) d_o^{\dagger}(k) \right) \tag{2.19b}$$

where we have taken the sum over $k > 0$ to simplify the Hamiltonian. Similarly we can write the Fourier transforms of the other fermionic terms: $c_{2i+1}^{\dagger} c_{2i}$, $c_{2i+1} c_{2i}$, $c_{2i+1}^{\dagger} c_{2i+2}$, $c_{2i+2}^{\dagger} c_{2i+1}$, $c_{2i+1}^{\dagger} c_{2i+2}^{\dagger}$, $c_{2i+2} c_{2i+1}$, $c_{2i}^{\dagger} c_{2i}$, and $c_{2i+1}^{\dagger} c_{2i+1}$. Plugging all these terms into the Hamiltonian (2.1.2) and rearranging it yields

$$H =$$

$$J \sum_{k>0} \left[\left\{ \alpha \left(d_e^{\dagger}(k) d_o(k) + d_o^{\dagger}(-k) d_e(-k) \right) + \beta \left(d_o^{\dagger}(-k) d_e^{\dagger}(k) + d_e(-k) d_o(k) \right) \right\} + h.c \right]$$

$$+ h \sum_{k>0} \left[d_e^{\dagger}(k) d_e(k) + d_e^{\dagger}(-k) d_e(-k) - d_o^{\dagger}(k) d_o(k) - d_o^{\dagger}(-k) d_o(-k) \right] \tag{2.20}$$

with $\alpha = (\cos k - i\delta \sin k)$ and $\beta = i\gamma \sin k$. For systems with more than one species of fermions it is convenient to use the Nambu formalism [42]. The single particle Hamiltonian (2.20) can be expressed in the following form

$$H = \sum_k \Psi_k^{\dagger} \mathcal{H}_k \Psi_k \tag{2.21}$$

where the Nambu spinor

$$\Psi_k^{\dagger} = \left(d_e^{\dagger}(k), d_o^{\dagger}(k), d_e(-k), d_o(-k) \right) \tag{2.22}$$

and the 4×4 Hamiltonian matrix is

$$\mathcal{H}_k = \begin{pmatrix} h & J\alpha & 0 & J\beta^* \\ J\alpha^* & -h & J\beta^* & 0 \\ 0 & J\beta & -h & -J\alpha \\ J\beta & 0 & -J\alpha^* & h \end{pmatrix} \tag{2.23}$$

2.2 Eigenvalues of the Hamiltonian

The spectrum with four energy bands can be obtained from diagonalization of the Hamiltonian matrix $\mathcal{H}_k$ given by Eq. (2.23). We use Mathematica [version 5.1.] for the matrix diagonalization, which yields four eigenvalues of the matrix $\mathcal{H}_k$:

$$\pm\epsilon^{\pm}(k) = \pm\sqrt{J^2\cos^2 k + \left(\sqrt{h^2 + J^2\delta^2\sin^2 k} \pm J\gamma\sin k\right)^2} \tag{2.24}$$

Now the Hamiltonian (2.21) has the diagonal form

$$H = \sum_{k,\alpha} \epsilon^{\alpha}(k)\eta^{\dagger}_{\alpha}(k)\eta_{\alpha}(k) \tag{2.25}$$

with $\alpha = 1, 2, 3, 4$. Here η_α are four eigen spinors.

In order to make the cross check of the obtained energy bands with the exactly solved known models we analyze the limiting cases:

(i) $h = 0$, there is no transverse magnetic field and the model reduces to the anisotropic dimerized XY model. The energy eigenvalues become

$$\pm\epsilon^{\pm}(k) = \pm J\sqrt{\cos^2 k + (\delta \pm \gamma)^2\sin^2 k} \tag{2.26}$$

and they are exactly the same as in Ref.[41].

(ii) $h = 0, \gamma = 0$; the model reduces to the well-known dimerized XY spin-1/2 chain. Eq. (2.24) gives the spectrum of this model:

$$\pm\epsilon^{\pm}(k) = \pm J\sqrt{\cos^2 k + \delta^2 \sin^2 k} \tag{2.27}$$

It was discussed in the section 1.1, of Eq. (1.11).

(iii) $h = 0, \delta = 0$; the model reduces to the anisotropic XY spin chain with two energy bands

$$\pm\epsilon^{\pm}(k) = \pm J\sqrt{\cos^2 k + \gamma^2 \sin^2 k}, \tag{2.28}$$

in exact agreement with the classical result [18].

By looking at the above limiting cases of the present model, we conclude that the eigenvalues (2.24) correctly recover other models studied in earlier literature.

To make another connection to the earlier related work we will present anisotropic dimerized XY spin-1/2 chain in the uniform transverse magnetic field. It has been proposed and solved in [41]. The resulting spectrum with four energy bands is

$$\pm\epsilon^{\pm}(k) =$$

$$\pm\sqrt{h^2 + J^2\cos^2 k + J^2(\delta^2+\gamma^2)\sin^2 k \pm 2J\sqrt{(J\delta\gamma\sin^2 k)^2 + h^2\left(\cos^2 k + \delta^2\sin^2 k\right)}} \tag{2.29}$$

2.3 Energy Gap and Quantum Criticality

From the Eq. (2.24) the energy gap of the spin system for $k = \pi/2$ can be found as

$$\Delta/J = \epsilon(k = \pi/2) = \sqrt{\left(\frac{h}{J}\right)^2 + \delta^2} \pm \gamma \tag{2.30}$$

The above Eq. (2.30) implies that for $\gamma = \pm\sqrt{(h/J)^2 + \delta^2}$ the system becomes

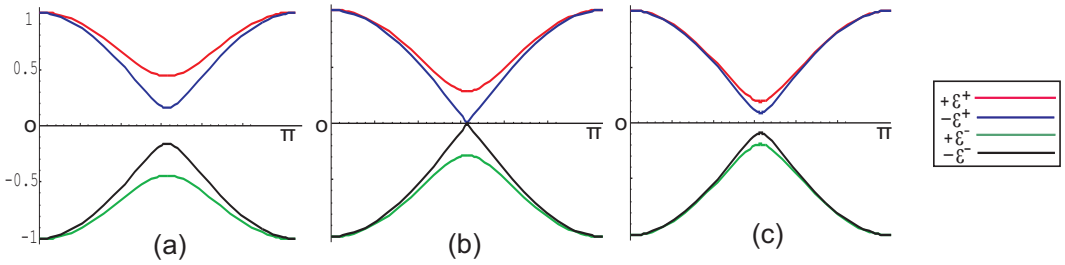

Figure 2.1: The four energy bands for different model's parameters (a) $\delta = 0.1, \gamma = 0.3, h = 0.1$; (b) $\delta = 0.1, \gamma = 0.141, h = 0.1$; and (c) $\delta = 0.1, \gamma = 0.05, h = 0.1$. The vertical axis is the energy and horizontal axis is the wavevector in the k space taken from 0 to π.

gapless and quantum critical. We illustrate this in Fig. 2.1. For $\gamma = +\sqrt{(h/J)^2 + \delta^2}$ there are two branches which become gapless at the some point, while the other two branches still remain gapped. Away from the quantum critical point $\gamma \neq \sqrt{(h/J)^2 + \delta^2}$ all four branches are gapped (massive).

In order to study the criticality of the model we rewrite the energy gap (2.30) in terms of the critical exponents:

$$\Delta/J \sim \mid t \mid^{\nu} \tag{2.31}$$

with $t = \sqrt{(h/J)^2 + \delta^2} - \gamma$ and $\nu = 1$. From the Eq. (2.31) we find the same critical exponent $\nu = 1$ for the gap Δ as in the 2D Ising model. The present model and the

2D Ising model are in the same universality class, since they both reduce to the free fermions.

To summarize:

In this chapter the antiferromagnetic anisotropic dimerized XY spin-1/2 chain in alternating transverse magnetic field is studied. In order to solve the model, the well-known 1D JWT was reviewed. It was found that this kind of transformation always preserves all spin commutation relations. By using it the spin operators were mapped onto spinless non-interacting fermionic operators. Then the free-fermionic Hamiltonian of two sub-lattices (odd and even) was mapped onto single particle Hamiltonian in momentum space by using the Nambu formalism. The spectrum of four energy bands was found by diagonalizing the single particle Hamiltonian using Mathematica. To know the critical behaviour of the model, the energy gap was obtained. It was shown that the model is quantum critical (massless) at some points and gapped (massive) otherwise. The present exactly solved model is in the same universality class as the 2D Ising model.

As we will show in the next chapter, the present model can be used to analyze the dimerized spin ladders in the free-fermionic approximation.

Chapter 3

Dimerized Two-leg Ladder

In this chapter the study focuses on dimerized two-leg ladders to understand its different quantum phases. To characterize the different phases we will calculate energy gaps, string order parameters and winding numbers. We will use the mean-field theory to treat treat the two-leg ladder.

The existence of a gap in spin ladders depends on the number of legs which is the special property of spin ladders. Ladders with m are gapped or gapless when m is even or odd, respectively. The even m-leg ladders are examples of spin liquids in which the formation of a gap is not due to the long range order or apparent symmetry breaking. The dimerized antiferromagnetic Heisenberg ladders are very interesting for studies of the hidden orders in quantum systems. It is known that single dimerized Heisenberg spin-1/2 chains are gapped [14] and if two chains are coupled into a ladder, the system is gapped even without dimerization [8]. On the other hand, it was conjectured in [44] that the dimerized two and three leg ladders can become gapless at some particular values in their couplings.

3.1 The Hamiltonian.

The dimerized ladder has two possible dimerization patterns on which two periodic couplings, i.e., strong $J(1+\delta)$ and weak $J(1-\delta)$ appear along the chains. The first has alternating couplings in each leg, called staggered dimerization pattern as in Fig. 3.1a. The second arranges each of parallel couplings to each leg, called columnar dimerization pattern as shown in Fig. 3.1b.

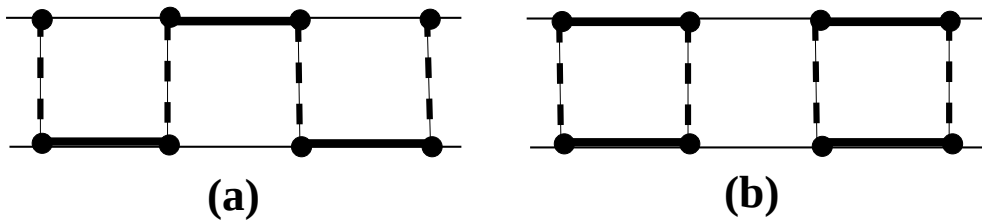

Figure 3.1: Dimerized two-leg ladder. The bold and/or thin and/or dashed lines represent the stronger and/or weaker chain couping $J(1+\delta)$ or $J(1-\delta)$ and rung coupling $J_\perp$, respectively. Dimerization patterns: (a) staggered and (b) columnar. Adapted from Ref.[45].

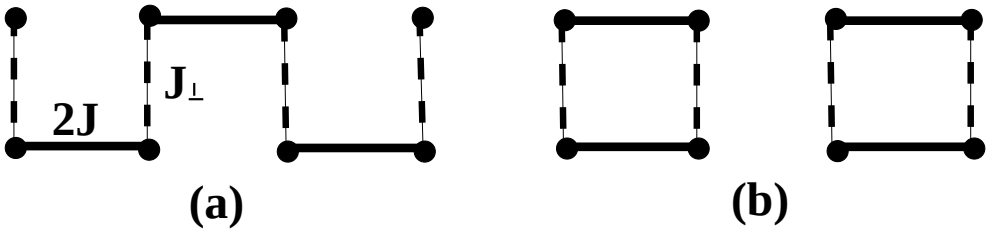

Figure 3.2: Completely dimerized ladder, $\delta = 1$. (a) Alternated stagering reduces model (3.2) to a snakelike dimerized Heisenberg chain of 2N spins. (b) Columnar order degenerates into a set of N/2 decoupled plaquettes. Adapted from Ref.[45].

Now we consider two possible dimerization ordering patterns of ladders: columnar and the staggered dimerization, which are defined as

$$J_\alpha(i) = J\left[1 + (-1)^{i+\alpha}\delta\right] \qquad \text{(staggered)} \qquad (3.1a)$$

$$J_\alpha(i) = J\left[1 + (-1)^i\delta\right] \qquad \text{(columnar)} \qquad (3.1b)$$

where $0 \leq \delta \leq 1$ is the dimerization parameter.

We write the Hamiltonian of the dimerized two-leg ladder with N rungs in the following form,

$$H = \sum_{\alpha=1}^{2}\sum_{i=1}^{N} J_\alpha(i)\mathbf{S}_\alpha(i)\mathbf{S}_\alpha(i+1) + J_\perp \sum_{i=1}^{N} \mathbf{S}_\alpha(i)\mathbf{S}_{\alpha+1}(i) \qquad (3.2)$$

We assume the situation when the dimerization only occurs along the chains ($\alpha = 1, 2$) for the constant rung coupling $J_\perp$. The total number of spins is $2N$.

At maximum dimerization, i.e, δ=1 the model (3.2) reduces to the snakelike chain [see Fig. 3.2a] in case of the staggered pattern and it shows the critical behaviour at $J_\perp = 2J$, and a set of decoupled plaquettes [see Fig. 3.2b] in the case of the columnar dimerization pattern.

We use the relation, $S_i^\alpha = \frac{1}{2}\sigma_i^\alpha$ with $\alpha = x, y, z$ and plug it into Eq. (3.2). Then it leads to,

$$H = \frac{1}{4}\sum_{i=1}^{N}\sum_{\alpha=1}^{2} J_\alpha(i)\left[\sigma_\alpha^x(i)\sigma_\alpha^x(i+1) + \sigma_\alpha^y(i)\sigma_\alpha^y(i+1) + \sigma_\alpha^z(i)\sigma_\alpha^z(i+1)\right]$$

$$+\frac{J_\perp}{4}\sum_{i=1}^{N}\left[\sigma_1^x(i)\sigma_2^x(i) + \sigma_1^y(i)\sigma_2^y(i) + \sigma_1^z(i)\sigma_2^z(n)\right] \qquad (3.3)$$

where σ_i^α are the Pauli spin operators in the ith site and α-th leg, and they obey the standard commutation relations.

To map the Hamiltonian (3.3) onto the system of spinless fermions we write the

particular form of the Jordan-Wigner transformation (JWT) as proposed in Ref.[46]:

$$\sigma_i^+ = c_i^+ \exp\left(i\pi \sum_{path,k=1}^{i-1} c_k^+ c_k\right) \tag{3.4}$$

where c_i is the fermi operator in the ith site, satisfies the following canonical anti-commutation relations.

$$\{c_i^+, c_j\} = \delta_{ij} \tag{3.5a}$$

and

$$\{c_i, c_j\} = \{c_i^+, c_j^+\} = 0 \tag{3.5b}$$

To use Eq. (3.4) into Eq. (3.3) we relabel all the sites of the two-leg ladder along the path described by Eq. (3.4) as shown in the Fig. 3.3. This path goes exactly through each lattice site only once. Here, substituting the relation

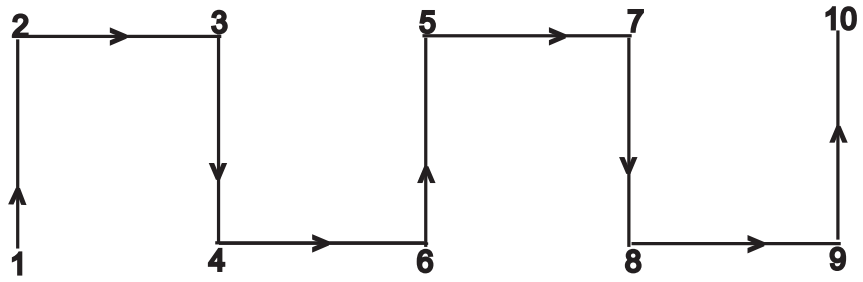

Figure 3.3: Schematics of the countour for the JWT that we use in the two leg ladder.

$\sigma_\alpha^\pm(i) = \left(\sigma_\alpha^x(i) \pm i\sigma_\alpha^y(i)\right)/2$ and using the JWT defined by Eq. (3.4), the Hamiltonian (3.3) becomes

$$H = \frac{1}{2}\sum_{i=1}^{N}\sum_{\alpha=1}^{2} J_\alpha(i)\left[c_\alpha^+(i)e^{i\phi_{\alpha(i,i+1)}}c_\alpha(i+1) + h.c + \left(n_\alpha(i) - \frac{1}{2}\right)\left(n_\alpha(i+1) - \frac{1}{2}\right)\right]$$

$$+\frac{1}{2}\sum_{i=1}^{N} J_{\perp}\left[c_1^{+}(i)c_2(i)+c_1(i)c_2^{+}(i)+\left(n_1(i)-\frac{1}{2}\right)\left(n_2(i)-\frac{1}{2}\right)\right] \tag{3.6}$$

where $n_\alpha(i) = c_\alpha^{+}(i)c_\alpha(i)$ is the particle number operator for ith site and $\phi_{\alpha(i,i+1)}$ is the phase difference between two lattice points i and $i+1$ for two leg ladder $\alpha = 1, 2$. By looking at the path given by JWT in Fig. 3.3, the phase differences at the different sites are as follows:

$$\phi_1(i_0) = \pi\left(n_2(i) + n_2(i+1)\right) \tag{3.7a}$$

$$\phi_2(i_e) = \pi\left(n_1(i) + n_1(i+1)\right) \tag{3.7b}$$

$$\phi_2(i_0) = 0, \qquad \phi_1(i_e) = 0 \tag{3.7c}$$

where i_e and i_o are even and odd lattice sites, respectively. In the ladder the magnetisation is not possible due to the strong fluctuations [8]. So, we can write $\langle S_\alpha^z(i)\rangle = \langle 1/2 - n_\alpha(i)\rangle = 0$ which gives $\langle n_\alpha(i)\rangle = 1/2$. We will use the mean field approximation such that the two particle interactions $\left(n_1(i)-\frac{1}{2}\right)\left(n_2(i)-\frac{1}{2}\right)$ are decoupled, and the approximate fermionic Hamiltonian contains only single particle terms. In this case there is an exact result due to Lieb [47] which states that phase per plaquette is π for half filled free fermions on a bipartite $2D$ lattice. Now, using this result in Eqs. (3.7a) and (3.7b) then we have the following relations:

$$(n_2(i) + n_2(i+1)) = 1 \tag{3.8a}$$

$$(n_1(i) + n_1(i+1)) = 1 \tag{3.8b}$$

We write π and 0 phases in the free fermionic terms of Eq. (3.6) and no extra phases occur along all rungs because the path of the JWT passes through all rungs as illustrated in Fig. 3.3. Thus we choose the configuration ....0-π-0..., and ....π-

0-π..., for IInd and Ist chains respectively as in Fig. 3.4. This π-flux phase (i.e.,

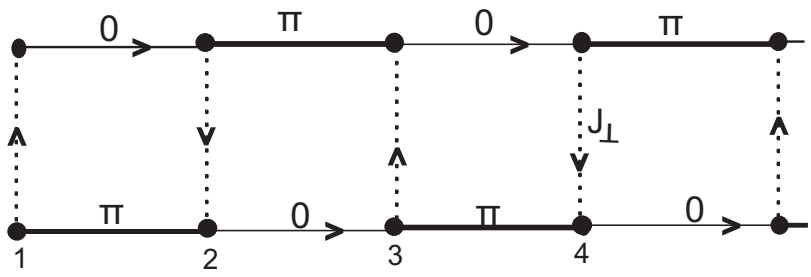

Figure 3.4: The phase per plaquette is equal to π.

configuration with π phase per plaquette) was found before Lieb from the mean-field analysis in earlier literature [48, 49], see also the book [2] for more references.

3.1.1 Mean Field Approximation

The interaction term of the Hamiltonian (3.6) is quartic in fermion operators. This type of problem can be treated by using the Mean Field Approximation (or Hartree-Fock Approximation) as explained in Ref. [2].

For instance, let us take an operator Q and it has an expectation value $\langle Q \rangle$ then we can write

$$Q = \langle Q \rangle + (Q - \langle Q \rangle) \tag{3.9}$$

where $(Q - \langle Q \rangle)$ is the fluctuation around its average. We can write similar equation for an operator Q' in terms of expectation value and fluctuation. Thus the product of the two operators gives,

$$QQ' = Q\langle Q' \rangle + \langle Q \rangle Q' - \langle Q \rangle \langle Q' \rangle + (Q - \langle Q \rangle)\,(Q' - \langle Q' \rangle) \tag{3.10}$$

In the Hartree-Fock approximation (MFA) we drop the fourth term in Eq. (3.10); the approximation consists of neglecting the fluctuations in second order. So, the

Hartree-Fock approximation is

$$QQ' \approx Q\langle Q'\rangle + \langle Q\rangle Q' - \langle Q\rangle\langle Q'\rangle \tag{3.11}$$

In the framework of MFA, we introduce two mean-field (i.e. effective hopping) parameters along the chain and rung defined, respectively, by

$$t_{\parallel}^{\alpha}(i) = -\langle c_{\alpha}^{+}(i)c_{\alpha}(i+1)\rangle \tag{3.12a}$$

$$t_{\perp} = -\langle c_{1}^{+}(i)c_{2}(i)\rangle \tag{3.12b}$$

Here the parameters along the chain could depend on the chain and rung number, but the rung parameter is assumed constant. This is due to the fact that the dimerization occurs along the chain only.

There is a quite extensive literature see, e.g. [50, 49, 46, 51, 45] and more references there on the mean-field approximations for treating the interacting terms in spin chains and ladders. We apply Hartree-Fock approximation on interacting fermion terms of Hamiltonian (3.6) by using the mean field equation (3.11) the the interacting fermionic terms can be expressed as

$$c_{\alpha}^{+}(i)c_{\alpha}(i)c_{\alpha}^{+}(i+1)c_{\alpha}(i+1) \approx c_{\alpha}^{+}(i)c_{\alpha}(i) + \left|t_{\alpha,\parallel}(i)\right|^{2}$$

$$+ \left(t_{\alpha,\parallel}^{*}(i)c_{\alpha}^{+}(i)c_{\alpha}(i+1) + h.c\right) \tag{3.13a}$$

$$c_{1}^{+}(i)c_{1}(i)c_{2}^{+}(i)c_{2}(i) \approx c_{1}^{+}(i)c_{1}(i) + \left(t_{\perp}^{*}c_{1}^{+}(i)c_{2}(i) + h.c\right) + \left|t_{\perp}\right|^{2} \tag{3.13b}$$

When we use Eqs. (3.13a) and (3.13b) for interacting terms in Eq. (3.6), we have

the following equations:

$$\left(n_\alpha(i)-\frac{1}{2}\right)\left(n_\alpha(i+1)-\frac{1}{2}\right)\approx\left(c_\alpha^+(i)c_\alpha(i+1)t^*_{\alpha,\|}(i)+h.c\right)+\left|t_{\alpha,\|}(i)\right|^2 \quad (3.14)$$

and,

$$\left(n_1(i)-\frac{1}{2}\right)\left(n_2(i)-\frac{1}{2}\right)\approx\left(c_1^+(i)c_2(i)t^*_{\perp}+h.c\right)+\left|t_{\perp}\right|^2 \quad (3.15)$$

Now we assume the phases of the free fermionic terms in Eq. (3.6) are as described by the π-flux arrangement in the Fig. 3.4, and we plug Eqs. (3.14) and (3.15) into Eq. (3.6). So it yields the quadratic Hamiltonian:

$$\begin{aligned}H=&\sum_{1=1}^{N}\left[\sum_{\alpha=1}^{2}J_\alpha(i)|t_{\alpha,\|}(i)|^2+J_\perp|t_\perp(i)|^2\right]\\&+\frac{1}{2}\sum_{i=1}^{N}\sum_{\alpha=1}^{2}\left[J_\alpha(i)(-1)^{i+\alpha-1}\left(c_\alpha^+(i)c_\alpha(i+1)+h.c\right)\right]\\&+\sum_{i=1}^{N}\sum_{\alpha=1}^{2}\left[J_\alpha(i)\left(c_\alpha^+(i)c_\alpha(i)t^*_{\alpha,\|}(i)+h.c\right)\right]\\&+\frac{J_\perp}{2}\sum_{i=1}^{N}\left[(1+2t^*_\perp)\left(c_1^+(i)c_2(i)+h.c\right)\right]\end{aligned} \quad (3.16)$$

Let us simplify Eq. (3.16) by further use of the Lieb result [47] for the π-flux of free fermionic Hamiltonian [see Fig 3.4]. We end up with the quadratic Hamiltonian:

$$\begin{aligned}H=&\frac{1}{2}\sum_{i=1}^{N}\sum_{\alpha=1}^{2}\left[J_{\alpha R}(i)(-1)^{i+\alpha-1}\left(c_\alpha^+(i)c_\alpha(i+1)+h.c\right)\right]\\&+\frac{J_{\perp R}}{2}\sum_{i=1}^{N}\left(c_1^+(i)c_2(i)+h.c\right)+H_0\end{aligned} \quad (3.17)$$

where,

$$H_0 = \sum_{i=1}^{N} \left[\sum_{\alpha=1}^{2} J_\alpha(i)|t_\parallel|^2 + J_\perp|t_\perp|^2 \right], \tag{3.18}$$

and

$$J_{\alpha R}(i) = J_\alpha(i)(1 + 2t_\parallel) \tag{3.19a}$$

$$J_{\perp R} = J_\perp(1 + 2t_\perp) \tag{3.19b}$$

are renormalized couplings along the chains ($\alpha = 1, 2$) and along the rungs, respectively.

To diagonalize the Hamiltonian we use the Fourier transform defined by the following relation

$$c_\alpha(2n+1) = \sqrt{\frac{2}{N}} \sum_k d_{\alpha o}(k) e^{-i(2n+1)k} \tag{3.20a}$$

$$c_\alpha(2n) = \sqrt{\frac{2}{N}} \sum_k d_{\alpha e}(k) e^{-i(2n)k} \tag{3.20b}$$

where $d_{\alpha,o}(k)$ and $d_{\alpha,e}(k)$ are Fourier transforms of fermi operators on the odd and even sites, respectively.

3.1.2 Staggered Dimerization

An illustration of the two-leg ladder in case of alternated staggered pattern is shown in Fig. 3.1a. It consists of two periodic strong $J(1+\delta)$ and weak $J(1-\delta)$ couplings along the chains. They couple with the rung coupling $J_\perp$ to form a ladder. We discuss the following limiting cases in the $(\delta, J_\perp)$ plane as studied in [45].

(i) If $\delta = 0$, i.e. no dimerization, then the model (3.2) reduces to the gapped uniform ladder for $J_\perp > 0$ and two decoupled gapless Heisenberg spin chains for $J_\perp = 0$.

(ii)If $\delta = 1$, i.e. maximum dimerization, then the model (3.2) becomes snakelike dimerized Heisenberg chain of $2N$ spins which becomes gapless when $J_\perp = 2J$: [See Fig. 3.2a].

To further simplify the Hamiltonian (3.17) in the staggered phase we plug Eqs. (3.1a), (3.20a) and (3.20b), into Eq. (3.17). The resulting Hamiltonian is of the following form:

$$H = J_R \sum_k \left[(i \sin k - \delta \cos k) \left(d^+_{1o}(k) d_{1e}(k) + d^+_{2e}(k) d_{2o}(k) \right) + h.c. \right]$$

$$+ \frac{J_{\perp R}}{2} \sum_k \left[\left(d^+_{1o}(k) d_{2o}(k) + d^+_{1e}(k) d_{2e}(k) \right) + h.c. \right] \tag{3.21}$$

After simplification of Eq. (3.21) we find the single particle effective Hamiltonian in the form of Eq. (2.21), where the Nambu spinor is

$$\Psi^\dagger(k) = \left(d^\dagger_{1e}(k), d^\dagger_{1o}(k), d^\dagger_{2e}(k), d^\dagger_{2o}(k) \right) \tag{3.22}$$

and the 4×4 Hamiltonian matrix

$$\mathcal{H}(k) = \begin{pmatrix} 0 & U & T & 0 \\ U^* & 0 & 0 & T \\ T & 0 & 0 & U^* \\ 0 & T & U & 0 \end{pmatrix}. \tag{3.23}$$

where we denote

$$U = -J_R \left(i \sin k + \delta \cos k \right) \qquad T = \frac{J_{\perp R}}{2} \tag{3.24a}$$

$$J_R = J(1 + 2t_\parallel) \qquad J_{\perp R} = J_\perp (1 + 2t_\perp) \tag{3.24b}$$

We use Mathematica to diagonalize (3.23), and find the eigenvalues of the Hamiltonian

$$\pm\epsilon^{\pm}(k) = \pm J_R \sqrt{\sin^2 k + \left(\delta \cos k \pm \frac{J_{\perp R}}{2J_R}\right)^2} \tag{3.25}$$

The spectrum of the Hamiltonian has an energy gap

$$\Delta = \epsilon(0) = J_R \left|\delta \pm \frac{J_{\perp R}}{2J_R}\right| \tag{3.26}$$

where $J_{\perp R}$ and J_R are the functions of $t_{\parallel}$ and $t_{\perp}$. From Eq. (3.26) we infer that the energy gap vanishes at $\delta = \pm J_{\perp R}/2J_R$.

We find the partition function Z for the single particle Hamiltonian (2.21) and the free energy per spin, as calculated in Ref. [45]. The latter is

$$f = \frac{F}{2N} = \frac{C_2}{2} - \frac{\log 2}{\beta} - \frac{1}{\beta\pi} \sum_{p=1}^{2} \int_0^{\frac{\pi}{2}} \ln \left[\cosh\left(\frac{\beta}{2}\epsilon_p(k)\right)\right] dk \tag{3.27}$$

where, β=$1/k_B T$, with Boltzmann constant k_B and

$$C_2 = 2J|t_{\parallel}|^2 + J_{\perp}|t_{\perp}|^2 \tag{3.28}$$

In the limit $T \to 0$ ($\beta \to \infty$) the Eq. (3.27) leads to the ground state energy per spin and reads as:

$$E_g = J|t_{\parallel}|^2 + \frac{J_{\perp}}{2}|t_{\perp}|^2 - \frac{1}{2\pi} \int_0^{\frac{\pi}{2}} (\epsilon_+(k) + \epsilon_-(k))\, dk \tag{3.29}$$

The minimization of the ground state energy with respect to $t_{\parallel}$ and $t_{\perp}$ gives two self-consistent equations and they are used to find the values of $t_{\parallel}$ and $t_{\perp}$. The

mean-field equations at zero temperature are

$$t_{\parallel} = \frac{1}{2\pi}\int_0^{\frac{\pi}{2}} \left(\frac{\sin^2 k + \delta^2 \cos^2 k + \frac{J_{\perp R}}{2J_R}\delta\cos k}{\sqrt{\sin^2 k + \left(\delta\cos k + \frac{J_{\perp R}}{2J_R}\right)^2}} \right) dk$$

$$+\frac{1}{2\pi}\int_0^{\frac{\pi}{2}} \left(\frac{\sin^2 k + \delta^2 \cos^2 k - \frac{J_{\perp R}}{2J_R}\delta\cos k}{\sqrt{\sin^2 k + \left(\delta\cos k - \frac{J_{\perp R}}{2J_R}\right)^2}} \right) dk \tag{3.30}$$

and,

$$t_{\perp} = \frac{1}{2\pi}\int_0^{\frac{\pi}{2}} \left(\frac{\delta\cos k + \frac{J_{\perp R}}{2J_R}}{\sqrt{\sin^2 k + \left(\delta\cos k + \frac{J_{\perp R}}{2J_R}\right)^2}} \right) dk$$

$$-\frac{1}{2\pi}\int_0^{\frac{\pi}{2}} \left(\frac{\delta\cos k - \frac{J_{\perp R}}{2J_R}}{\sqrt{\sin^2 k + \left(\delta\cos k - \frac{J_{\perp R}}{2J_R}\right)^2}} \right) dk \tag{3.31}$$

The mean field parameters $t_{\parallel}$ and $t_{\perp}$ renormalize the hopping in the free-fermionic Hamiltonian (3.17) and are implicitly defined by Eqs. (3.30) and (3.31). Here we are interested to determine $t_{\parallel}$ and $t_{\perp}$ at the different values of dimerization parameter δ and rung coupling $J_{\perp}$.

First we are going to find the behaviour of $t_{\parallel}$ and $t_{\perp}$ in the following limiting cases.

(A) $\delta = 0$ (Uniform Ladder)

(B)$J_{\perp} = 0$ (Dimerized Chain)

(C)$\delta = 1$ (Completely Dimerized Ladder)

Now, we discuss the different limiting cases in the detail.

(A) $\delta = 0$ (Uniform Ladder)

In the uniform ladder the mean field parameters $t_\parallel$ and $t_\perp$ have been analysed in [49, 52, 53] with respect to the rung coupling $J_\perp$. First we analyze their behaviour independently and then they will be compared to the results of [53].

For this we integrate Eqs. (3.30) and (3.31) to obtain

$$t_\parallel = \frac{1}{\pi}\left[\sqrt{a^2+1}\mathbf{E}\left(\frac{1}{a^2+1}\right) - \frac{a^2}{\sqrt{a^2+1}}\mathbf{K}\left(\frac{1}{a^2+1}\right)\right] \tag{3.32}$$

$$t_\perp = \frac{1}{\pi}\left[\frac{a}{\sqrt{a^2+1}}\mathbf{K}\left(\frac{1}{a^2+1}\right)\right], \tag{3.33}$$

where $\mathbf{K}$ and $\mathbf{E}$ are elliptic integrals of first and second kind respectively, and

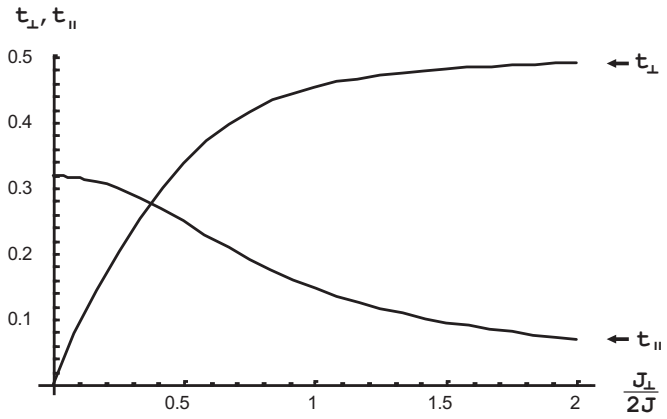

Figure 3.5: The mean-field parameters $t_\parallel$ and $t_\perp$ as functions of $J_\perp/2J$ for $\delta = 0$.

$$a \equiv \frac{J_{\perp R}}{2J_R} = \frac{J_\perp(1+2t_\perp)}{2J(1+2t_\parallel)} \tag{3.34}$$

is an auxiliary parameter. Now, Eq. (3.32) and (3.33) can be solved numerically for different values of $J_\perp/2J$ and their behaviour is displayed in Fig. 3.5.

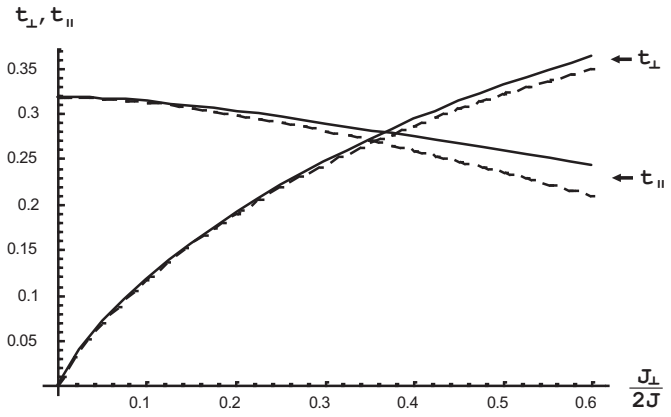

Figure 3.6: $t_{\parallel}$ and $t_{\perp}$ as functions of $J_{\perp}/2J$ from Eq. (3.30) and (3.31) and dashed lines are approximate analytic results (3.35) and (3.36) for $J_{\perp}/2J \ll 1$ for $\delta = 0$.

We can expand the functions **E** and **K** to leading order.

For $\frac{J_{\perp}}{2J} \ll 1$ we find

$$t_{\parallel} \approx \frac{1}{\pi} - \frac{1}{2\pi}\left(\frac{J_{\perp}/2J}{(1+2/\pi)}\right)^2 \log\left(\frac{(1+2/\pi)}{J_{\perp}/2J}\right) \tag{3.35}$$

$$t_{\perp} \approx \frac{1}{\pi}\left(\frac{J_{\perp}/2J}{(1+2/\pi)}\right) \log\left(\frac{4(1+2/\pi)}{J_{\perp}/2J}\right) \tag{3.36}$$

For $\frac{J_{\perp}}{2J} \gg 1$,

$$t_{\parallel} \approx \frac{1}{\left(8\frac{J_{\perp}}{2J} - 2\right)} \tag{3.37}$$

$$t_{\perp} \approx \frac{1}{2} - \frac{1}{2}\left(\frac{1}{\left(4\frac{J_{\perp}}{2J} - 1\right)}\right)^2 \tag{3.38}$$

From Fig. 3.6 and 3.7 we conclude that, approximate results have good agreement with the numerical solution for $J_{\perp}/2J < 0.3$ and $J_{\perp}/2J > 1.5$ respectively. The numerical and analytical results which we find here for both limiting cases (i.e.,

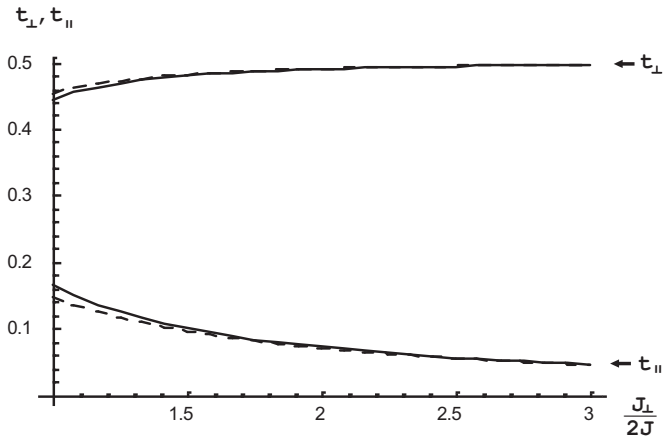

Figure 3.7: $t_{\|}$ and $t_{\perp}$ as functions of $J_{\perp}/2J$ from Eqs. (3.30) and (3.31) and dashed lines are approximate analytic results (3.37) and (3.38) for $J_{\perp}/2J \gg 1$ for $\delta = 0$.

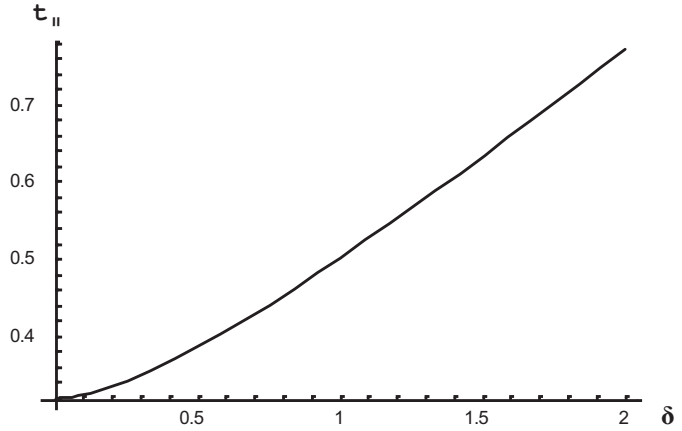

Figure 3.8: $t_{\|}$ as a function of δ at $J_{\perp}$=0.

$J_{\perp}/2J \gg 1$ and $J_{\perp}/2J \ll 1$), were obtained in [53].

(B) $J_{\perp} = 0$ (Dimerized Chain)

In this case we find the behaviour of mean-field parameters in a single dimerized chain. From Eqs. (3.30) and (3.31) we have a straightforward result that $t_{\perp} = 0$ and $t_{\|}$ is a function of δ, is given by

$$t_{\|} = \frac{\delta}{\pi}\mathbf{E}\left[1 - \frac{1}{\delta^2}\right] \tag{3.39}$$

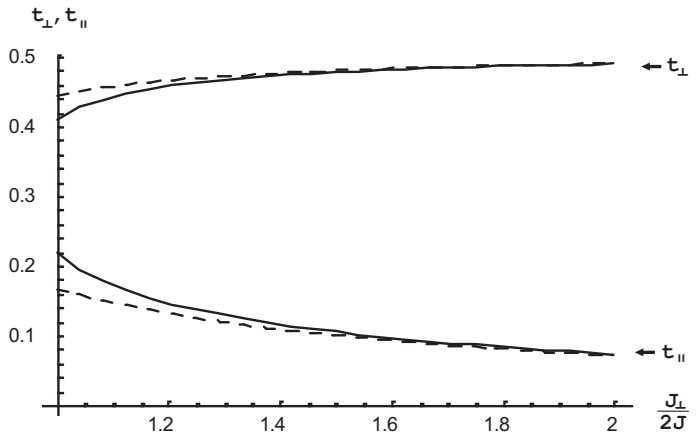

Figure 3.9: $t_{\|}$ and $t_{\perp}$ as functions of $J_{\perp}/2J$ at $\delta = 1$ from Eqs. (3.30) and (3.31) and dashed lines are approximate analytic results (3.42) and (3.43) for $J_{\perp}/2J > 1$.

We plot $t_{\|}(\delta)$ in Fig. 3.8 and find that it grows smoothly from origin.

(C) $\delta = 1$ (Completely Dimerized Ladder)

In the maximum dimerization the dimerized ladder reduces to the snakelike dimerized Heisenberg spin chain which becomes gapless when $J\perp = 2J$.

For $\frac{J_{\perp}}{2J} \ll 1$, we integrate Eq. (3.30) and (3.31) and expand the functions to the leading order for the following two limiting cases. We find the parameters

$$t_{\|} = \frac{1}{2} - \frac{1}{2}\left(\frac{J_{\perp}/2J}{4 - J_{\perp}/2J}\right)^2 \tag{3.40}$$

$$t_{\perp} = \frac{1}{2}\left(\frac{J_{\perp}/2J}{4 - J_{\perp}/2J}\right) \tag{3.41}$$

For $\frac{J_{\perp}}{2J} \gg 1$,

$$t_{\|} = \frac{1}{(8\frac{J_{\perp}}{2J} - 2)} \tag{3.42}$$

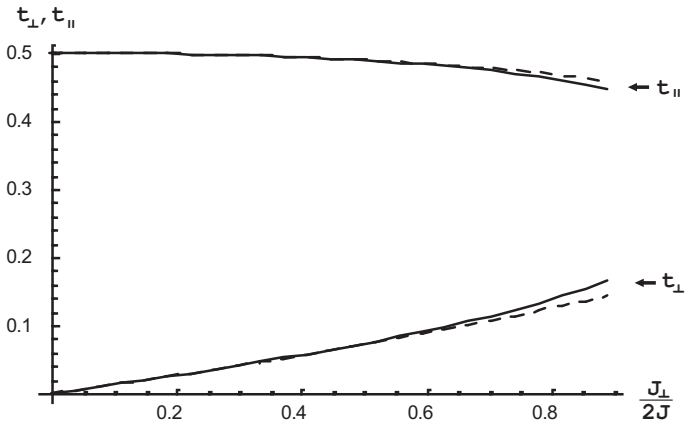

Figure 3.10: $t_{\|}$ and $t_{\perp}$ as functions of $J_{\perp}/2J$ at $\delta = 1$ from Eqs. (3.30) and (3.31) and dashed lines are approximate analytic results (3.40) and (3.41) for $J_{\perp}/2J < 1$.

$$t^{\perp} = \frac{1}{2} - \frac{1}{2}\left(\frac{1}{(4\frac{J_{\perp}}{2J} - 1)}\right)^2 \tag{3.43}$$

From Fig. 3.9 and 3.10 we conclude that approximate analytic results have good agreement with the numerical results for $J_{\perp}/2J > 1.4$ and $J_{\perp}/2J < 0.7$, respectively.

Now we will discuss the behaviour of $t_{\|}$ and $t_{\perp}$ in the staggered dimerized ladder in the whole range of model's parameters. Here we have to point out that the mean-field Eqs. (3.30) and (3.31) follow as a special case from the results of the slightly more sophisticated mean-field analysis of Ref. [45]. They can be derived from the equations presented in that paper after some simplifications. However the present mean-field equations are much simpler, while the hopping parameters, ground state energies and the gaps have only small numerical differences with the corresponding results of Ref.[45]. The same applies for the columnar phase considered in the following section. The version of the mean-field approximation presented here results in essentially the same physical predictions for the two-leg ladder as in the earlier

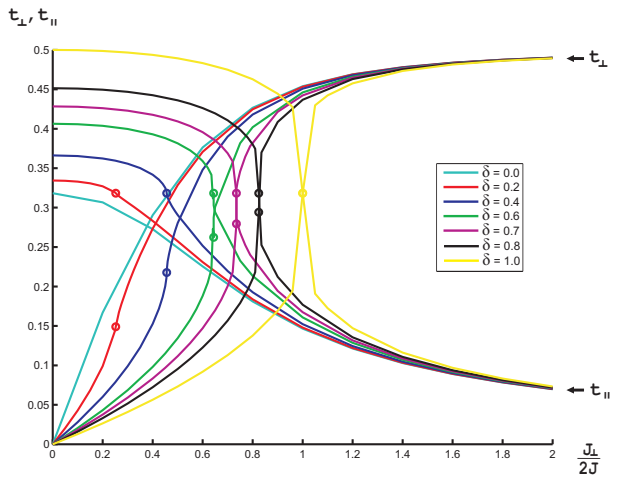

Figure 3.11: $t_{\|}$ and $t_{\perp}$ are functions of $J_{\perp}/2J$ and circles are the points where gap exactly vanishes corresponding to different δ.

analysis [45] and the simple free-fermionic Hamiltonian (3.17) is very useful for the analytical treatments of the model and can be used for getting more analytic results [54].

As we discussed before, $t_{\|}$ and $t_{\perp}$ as functions of $J_{\perp}/2J$ and δ are determined by Eqs. (3.30) and (3.31). The analytical treatment is not possible to study the behaviour of $t_{\|}$ and $t_{\perp}$ in the whole parameter space $(\delta, J_{\perp}/2J)$. So, we resort to numerical methods for this purpose. We used Mathematica to find the numerical solution of (3.30) and (3.31). The numerical solutions are found to be unstable and oscillating quickly in the vicinity of vanishing gap. We identify the origin of the problem: the equations have multiple roots in this region. The problem is resolved by taking the suitable root that provides the minimum ground state energy. We plot the dependencies of $t_{\|}$ and $t_{\perp}$ to $J_{\perp}/2J$ for different values of δ: See. Fig. 3.11. In the vicinity of Quantum Critical Point (QCP) or (vanishing gap) we took few discrete points. From Eqs. (3.30), (3.31), (3.26), and (3.34) we find that the energy gap varies in the parametric space $(J_{\perp}/2J, \delta)$. We plot the gap as the function of

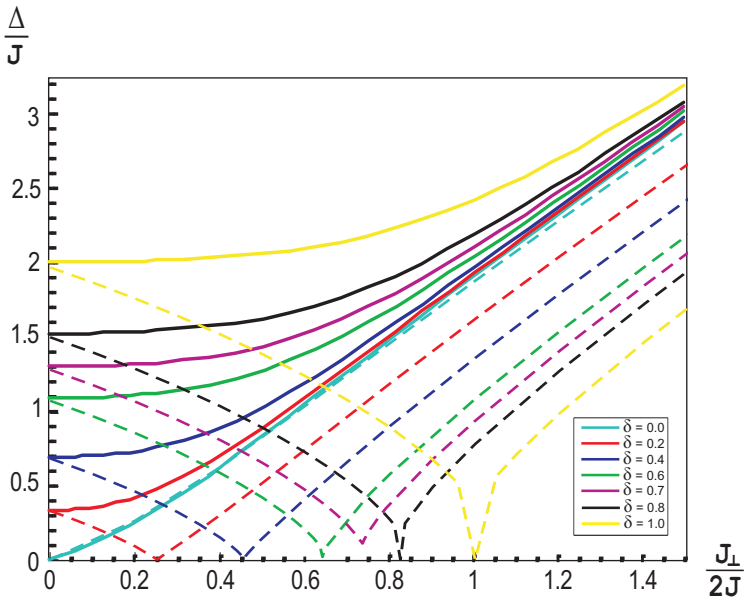

Figure 3.12: The gaps of two-leg ladder in the staggered and columnar phases. For a fixed dimerization δ the gaps of staggered (dashed lines) and columnar (solid lines) configurations coincide only at $J_\perp = 0$. The columnar gap grows monotonously with $J_\perp/2J$, while the staggered gap demonstrates critical behaviour and vanishes at the critical point. The gap in the uniform ladder ($\delta = 0$) is also shown for the comparision.

$J_\perp/2J$ for different values of δ in Fig. 3.12. The figure shows that the gap changes smoothly with respect to $J_\perp/2J$ for each value of δ by showing the critical behaviour at different points on the $J_\perp/2J$ axis.

In the range of dimerization parameter $0.45 \leq \delta \leq 0.75$ the multiple roots of the mean-field equations occur and the small residual gap is found. The region with the residual gap is shown by the dashed line of the critical line in the phase diagram Fig. 3.13. This small residual gap (i.e. weak first order phase transition, see also jumps in the hopping parameters in Fig. 3.11) occurs only in some parts of the critical line. It is clearly an artefact of the mean-field approximation, since more sophisticated

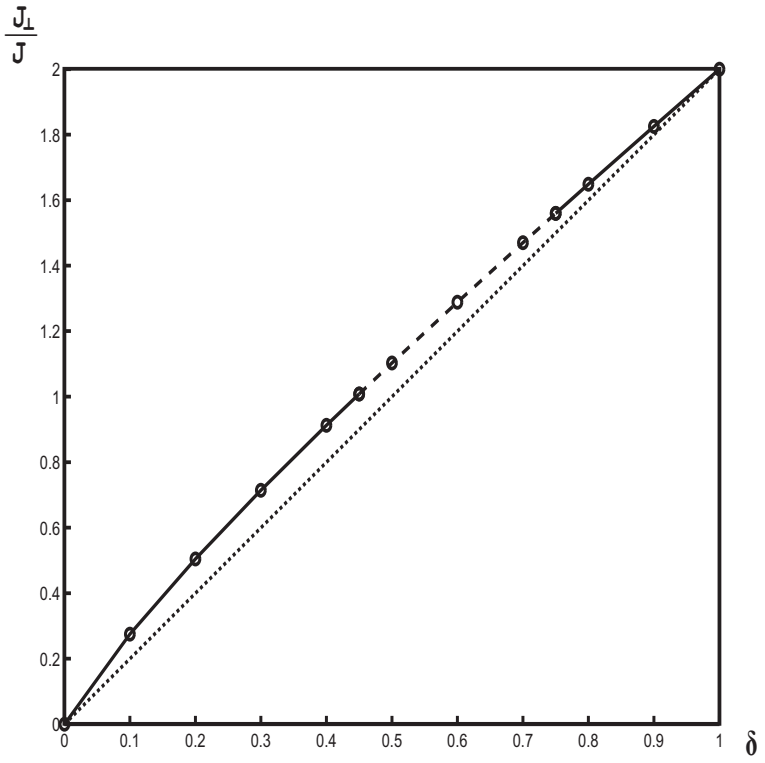

Figure 3.13: Phase diagram of the staggered phase. The solid line is the critical line where gap vanishes (i.e., the critical line between two phases), and the dashed line indicates the part of the phase boundary where a small residual gap exists. The dotted straight is guide for an eye.

earlier treatments of the same model, mainly numerical, [55, 56, 57, 58, 59, 60] indicate clearly a continuous phase transition. The phase diagram shown in Fig. 3.13 is virtually indistinguishable from the diagram given by a different version of the MFA [45].

Finally, we briefly study the critical behaviour in this phase of the ladder near to the quantum critical lines $\delta_c = \pm J_{\perp R}/2J_R$ by using the critical exponents. Now we write Eq. (3.26) as

$$\frac{\Delta_s}{J_R} \sim \mid \delta - \delta_c \mid^{\nu} \tag{3.44}$$

with $\nu = 1$. Here we find the exponent $\nu = 1$ for the gap Δ as in the 2D Ising model. As it must, the free-fermionic treatment of the two-leg ladder in the staggered phase results in the critical universality class of the 2D Ising model.

3.1.3 Columnar Dimerization

An illustration of the two-leg ladder in case of the columnar dimerization pattern is shown in Fig. 3.1b. It consists of two couplings: strong $J(1+\delta)$ and weak $J(1-\delta)$, such that strong/weak links on each of the legs are arranged parallel to each other. We discuss the following limiting cases in $(\delta, J_\perp)$ plane as studied in [45].

(i) If $\delta = 0$, i.e. no dimerization (columnar of staggered), then the model (3.2) reduces to a gapped uniform ladder for $J_\perp > 0$ and two decoupled gapless Heisenberg spin chains for $J_\perp = 0$.

(ii)If $\delta = 1$, i.e. maximum dimerization, then the model (3.2) becomes a set of $N/2$ decoupled four-spin plaquettes: [See Fig. 3.2b].

Here we consider the columnar dimerization pattern in a ladder as displayed in Fig. 3.1b. By using Eqs. (3.1b), (3.20a) and (3.20b) for the Hamiltonian (3.17) we get

$$H = J_R \sum_k \left[(i \sin k + \delta \cos k) \left(d^+_{1o}(k) d_{1e}(k) + d^+_{2e}(k) d_{2o}(k) \right) + h.c \right]$$
$$+ \frac{J_{\perp R}}{2} \sum_k \left[\left(d^+_{1o}(k) d_{2o}(k) + d^+_{1e}(k) d_{2e}(k) \right) + h.c \right] \tag{3.45}$$

After simplification of Eq. (3.45),we find the single particle effective Hamiltonian as in Eq. (2.21) with the same spinor defined in (3.22) and the 4×4 Hamiltonian

matrix:

$$H_d(k) = \begin{pmatrix} 0 & U_+ & T & 0 \\ U_+^* & 0 & 0 & T \\ T & 0 & 0 & U_-^* \\ 0 & T & U_- & 0 \end{pmatrix} \tag{3.46}$$

where $U_\pm = J_R\left(-i\sin(k) \pm \delta\cos(k)\right)$ and $T = J_{\perp R}/2$. Diagonalization of Eq. (3.46) results in the two doubly degenerate Hamiltonian eigenvalues

$$\pm\epsilon^{\pm}(k) = \pm J_R\sqrt{\sin^2 k + \delta^2\cos^2 k + \left(\frac{J_{\perp R}}{2J_R}\right)^2} \tag{3.47}$$

Thus the energy gap is

$$\Delta = \epsilon(0) = J_R\sqrt{\delta^2 + \left(\frac{J_\perp R}{2J_R}\right)^2} \tag{3.48}$$

indicating that the columnar phase is always gapped, in agreement with the earlier result of Ref. [45]. In this sense the columnar phase is qualitatively similar to the uniform ladder. The gap persists in the limit of two decoupled chains $J_\perp \to 0$, giving $\Delta_c = J_R\delta$ as it must be for the single spin chain in the XY-free-fermionic approximation. The gap disappears only together with the vanishing chain dimerization $\delta \to 0$ in agreement with the result for the uniform chain.

By calculating the partition function of the single particle Hamiltonian as explained above for the case of the staggered phase, the free energy per spin is given by an equation similar to Eq. (3.27). The ground state energy per spin reads as:

$$E_g = J|t_\parallel|^2 + \frac{J_\perp}{2}|t_\perp|^2 - \frac{1}{\pi}\int_0^{\frac{\pi}{2}} \epsilon(k)dk \tag{3.49}$$

Minimization of the ground state energy with respect to $t_{\parallel}$ and $t_{\perp}$ gives two self-consistent equations and they are used to find the values of $t_{\parallel}$ and $t_{\perp}$. The mean-field equations at zero temperature are

$$t_{\parallel} = \frac{1}{\pi}\int_0^{\frac{\pi}{2}} \left(\frac{\sin^2 k + \delta^2 \cos^2 k}{\sqrt{\sin^2 k + \delta^2 \cos^2 k + \left(\frac{J_{\perp R}}{2J_R}\right)^2}} \right) dk \tag{3.50}$$

and,

$$t_{\perp} = \frac{1}{\pi}\int_0^{\frac{\pi}{2}} \left(\frac{\frac{J_{\perp R}}{2J_R}}{\sqrt{\sin^2 k + \delta^2 \cos^2 k + \left(\frac{J_{\perp R}}{2J_R}\right)^2}} \right) dk \tag{3.51}$$

Here, we are interested to determine the renormalization parameters $t_{\parallel}$ and $t_{\perp}$ in the parametric region $(J_{\perp}/2J, \delta)$. By comparing the mean field Eqs. (3.30) and (3.31) of staggered phase and Eqs. (3.50) and (3.51) of columnar phase we find the same behaviour in the limiting cases $\delta \to 0$ and $J_{\perp}/2J \to 0$ because the two ladders (staggered and columnar) coincide to each other in these limits. The analytic and numerical study of these parameters can be found in subsection 3.1.2 . An analytic treatment is not possible to study the behaviour of the renormalization parameters $t_{\parallel}$ and $t_{\perp}$ in the whole parametric region $(J_{\perp}/2J, \delta)$, as in the case of staggered phase. We find these parameters numerically. They vary continuously in the whole region. The columnar phase has no phase transition and no gap vanishing region. We plot $t_{\parallel}$ and $t_{\perp}$ as functions of $J_{\perp}/2J$ for different values of δ in Fig. 3.14. From Eqs. (3.34), (3.50), (3.51) and (3.48), we find that the energy gap varies smoothly in the parametric space $(J_{\perp}/2J, \delta)$. We plot the gap as a function of $J_{\perp}/2J$ for different values of δ in Fig. 3.12. The figure demonstrates that the gap in the columnar phase (solid lines) increases continuously and monotonously with respect

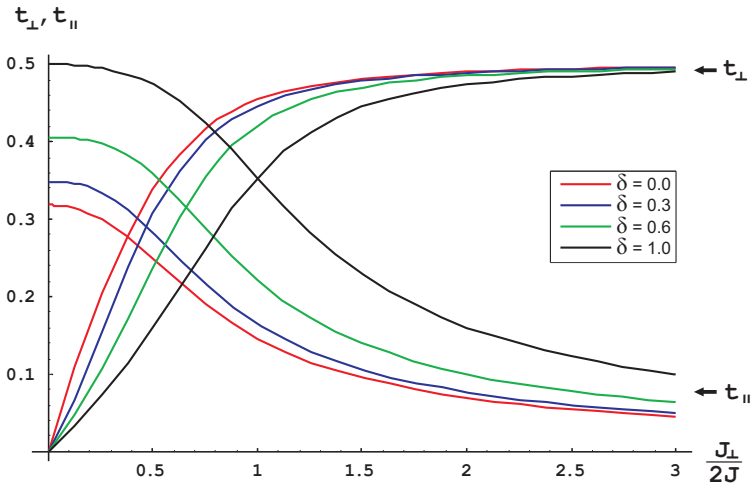

Figure 3.14: $t_{\|}$ and $t_{\perp}$ as functions of $J_{\perp}/2J$ in the different dimerization parameter δ.

to $J_{\perp}/2J$ for each value of δ. In Fig. 3.12 the gaps of the staggered and columnar phases are plotted as functions of $J_{\perp}/2J$ for different dimerizations.

To summarize:

In this chapter, the antiferromagnetic dimerized Heisenberg two-leg spin ladder with two possible dimerization patterns was studied. By using the JWT we mapped spin operators onto spinless fermionic operators. The interacting fermionic terms appeared in the Hamiltonian were decoupled into single-particle terms within the mean-field approximation (MFA). By using the Fourier transform and the Nambu formalism we obtained the single particle Hamiltonian and its eigenvalues were found by using Mathematica. Then the mean-field equations were obtained from the minimization of the ground state energy. At first, they were analyzed by numerical and analytical methods in the limits in parametric $(J_{\perp}/2J, \delta)$ space. All above mentioned calculations were done for both the staggered and columnar dimerization configurations. In both phases it was noticed that there were good qualitative and quantitative agreements with the previous results obtained in Ref [45].

The mean-field equations were analyzed numerically by using Mathematica in the whole parameter space $(J_\perp/2J, \delta)$. In the staggered phase these equations were unstable in some regions of the parameter space near the quantum criticality. We noticed and calculated the residual gap near the critical points. The columnar phase remains consistently gapped and all parameters in that phase vary smoothly. We attribute this residual gap to the artefact of the MFA.

On the other hand, by looking at the similar spectra Eqs. (3.25) and (2.24) the staggered phase of the two-leg ladder can be mapped onto the anisotropic XY model in a transverse magnetic field. For this purpose the parameters of both models are related as follows;

$$J_R \to J, \quad \delta \to \gamma, \quad \frac{J_{\perp R}}{2} \to h, \quad \text{and} \quad k \to \left(\frac{\pi}{2} - k\right) \tag{3.52}$$

From the similar spectra Eqs. (3.47) and (2.24) we can map the columnar phase of two-leg ladder onto the dimerized XY model in an alternating transverse magnetic field. In this mapping the parameters of the models are related as follows:

$$J_R \to J, \quad \delta \to \delta, \quad \frac{J_{\perp R}}{2} \to h, \quad \text{and} \quad k \to \left(\frac{\pi}{2} - k\right) \tag{3.53}$$

The above mentioned two mapped spin models of the staggered and columnar phases of two-leg ladder are very useful for further analyzing the topological phases and getting more analytical result [54].

Chapter 4

String Order Parameter in Spin Chains

4.1 SOP in Dimerized XY Chain

We consider an antiferromagnetic dimerized XY spin chain where the exchange coupling coefficients J_i alter at odd and even sites as shown in the Fig. 4.1. The exchange coupling is written as

$$J_i = J\left(1 + (-1)^i \delta\right) \tag{4.1}$$

where i is the lattice site of the spin chain, and δ is called the dimerization parameter.

Figure 4.1: A spin chain with an alternation of strong and weak bonds adapted from [14].

The Hamiltonian of the dimerized XY chain is written in terms of the Pauli matrices as

$$H = \frac{J}{4}\sum_{i=1}^{N}\left[\left(1+(-1)^i\delta\right)\sum_{\alpha=x,y}\sigma_i^\alpha\sigma_{i+1}^\alpha\right] \tag{4.2}$$

Dividing explicitly the chain into the even and odd sites, the Hamiltonian reads:

$$H = \frac{J}{4}\sum_{i=1}^{N/2}\left[(1+\delta)\left(\sigma_{2i}^x\sigma_{2i+1}^x+\sigma_{2i}^y\sigma_{2i+1}^y\right)+(1-\delta)\left(\sigma_{2i+1}^x\sigma_{2i+2}^x+\sigma_{2i+1}^y\sigma_{2i+2}^y\right)\right] \tag{4.3}$$

We now apply the duality transformation (1.23a) and (1.23b). This transformation was proposed by Fradkin and Susskind [29], and recently its version was applied in Ref.[68] to study the SOP in the Kitaev model. Using this transformation in the terms $\sigma_{2i}^x\sigma_{2i+1}^x$ and $\sigma_{2i}^y\sigma_{2i+1}^y$, we find

$$\sigma_{2i}^x\sigma_{2i+1}^x = \tau_{2i-1}^x\tau_{2i}^x\tau_{2i}^x\tau_{2i+1}^x = \tau_{2i-1}^x\tau_{2i+1}^x \tag{4.4}$$

and

$$\sigma_{2i}^y\sigma_{2i+1}^y = \prod_{k=2i}^{N}\tau_k^y\prod_{k=2i+1}^{N}\tau_k^y = \tau_{2i}^y \tag{4.5}$$

Similarly we apply the duality transforamtion for the terms $\sigma_{2i+1}^x\sigma_{2i+2}^x$ and $\sigma_{2i+1}^y\sigma_{2i+2}^y$ and get the Hamiltonian (4.3) in terms of the dual operators:

$$H = \frac{J}{4}\sum_{i=1}^{N}\left[(1+\delta)\tau_{2i-1}^x\tau_{2i+1}^x+(1-\delta)\tau_{2i+1}^y\right]+\left[(1-\delta)\tau_{2i}^x\tau_{2i+2}^x+(1+\delta)\tau_{2i}^y\right] \tag{4.6}$$

The Hamiltonian (4.6) consists of two decoupled 1D Ising models in transverse field. Similar transformations were also studied in Ref. [61, 23]. One of the models resides on the odd dual lattice sites, and the other on the even sites as illustrated in Fig. 4.2. So we can write

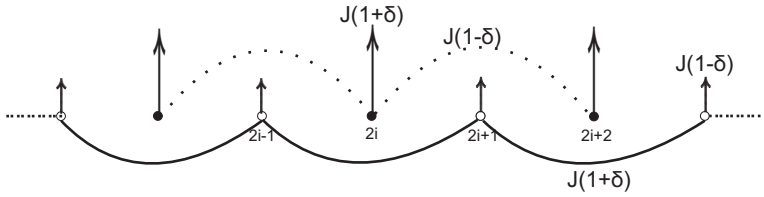

Figure 4.2: Odd and even decoupled Ising chains in transverse field on the dual lattice.

$$H_o = \frac{J}{4}\sum_{i=1}^{N}\left[(1+\delta)\tau_{2i-1}^{x}\tau_{2i+1}^{x} + (1-\delta)\tau_{2i+1}^{y}\right] \tag{4.7a}$$

$$H_e = \frac{J}{4}\sum_{i=1}^{N}\left[(1-\delta)\tau_{2i}^{x}\tau_{2i+2}^{x} + (1+\delta)\tau_{2i}^{y}\right] \tag{4.7b}$$

and the total Hamiltonian (4.6) becomes $H = H_o + H_e$.

Pfeuty [62] was the first to derive the correlation function $\left\langle \sigma_1^x \sigma_{l+1}^x \right\rangle$ of the 1D Quantum Ising model (QIM) with the Hamiltonian

$$H = \sum_{i=1}^{N}\left[\frac{\widetilde{J}}{4}\sigma_i^x\sigma_{i+1}^x + \frac{h}{2}\sigma_i^z\right] \tag{4.8}$$

According to results of Pfeuty and McCoy [62, 64] the correlation function can be written as

$$\lim_{l\to\infty}\left\langle \sigma_i^x\sigma_{i+l}^x\right\rangle = (-1)^l\left(1-\lambda^{-2}\right)^{\frac{1}{4}} = (-1)^l m_x^2 \tag{4.9}$$

for $\lambda \equiv \widetilde{J}/2h > 1$, and m_x vanishes when $\lambda \leq 1$.

Let us recall that the $1D$ QIM is ordered for $\lambda > 1$ and disordered for $\lambda \leq 1$. The limit of the spin-spin correlation function (4.9) signals the appearance of the long-range order (LRO) m_x. To work with correlation functions of the τ's operators let us compare the Hamiltonian (4.7a) with the $1D$ QIM Hamiltonian (4.8). Then

we can identify

$$\widetilde{J} \longleftrightarrow J(1+\delta) \tag{4.10a}$$

$$h \longleftrightarrow \frac{J}{2}(1-\delta) \tag{4.10b}$$

to obtain

$$\lambda \equiv \frac{\widetilde{J}}{2h} = \frac{1+\delta}{1-\delta} > 1 \tag{4.11}$$

for $\delta > 0$. Thus the Hamiltonian H_o has LRO $\langle \tau^x \rangle \neq 0$ in the ground state. Using (4.11) in (4.9) for the correlation function of τ-operators, we obtain

$$\begin{aligned} \lim_{l\to\infty} \langle \tau_0^x \tau_l^x \rangle &= (-1)^l \left[1 - \left(\frac{1-\delta}{1+\delta} \right)^2 \right]^{\frac{1}{4}} \\ &= (-1)^l \left[\frac{4\delta}{(1+\delta)^2} \right]^{\frac{1}{4}} \end{aligned} \tag{4.12}$$

Thus the $\langle \tau_l^x \rangle$ can be regarded as a conventional (local) order parameter in the dual space. Combining Eqs. (4.12) and (1.34) for odd sites sites we obtain exact result for the SOP; which characterizes the hidden topological order.

$$O_o^x = \begin{cases} \frac{1}{4}\left[\frac{4\delta}{(1+\delta)^2} \right]^{\frac{1}{4}} & \delta > 0 \\ 0 & \delta \leq 0 \end{cases} \tag{4.13}$$

Equation (4.13) indicates that there is no odd string order at $\delta \leq 0$ because dual spins τ_l^x residing on the odd sites are disordered in this case.

Similarly, let us compare the even Hamiltonian (4.7b) and the 1D QIM (4.8). In this case we find

$$\widetilde{J} \longleftrightarrow J(1-\delta) \tag{4.14a}$$

$$h \longleftrightarrow \frac{J}{2}(1+\delta) \tag{4.14b}$$

Using the McCoy's result (4.9) for the correlation function of τ^x on even sites we find that the even lattice spins τ^x are ordered in the case $\delta < 0$ and disordered at $\delta \geq 0$. So the original spin Hamiltonian (4.2) has hidden topological order characterized by the even string order parameter

$$O_e^x = \begin{cases} \frac{1}{4}\left[\frac{-4\delta}{(1-\delta)^2}\right]^{\frac{1}{4}} & \delta < 0 \\ 0 & \delta \geq 0 \end{cases} \tag{4.15}$$

From Eqs. (4.13) and (4.15) we can write the common formula for the non-vanishing SOP's as follows:

$$O_o^x(\delta) = O_e^x(-\delta) = \frac{1}{4}\left[\frac{4|\delta|}{(1+|\delta|)^2}\right]^{\frac{1}{4}} \tag{4.16}$$

From Eq. (4.16) we plot the odd and even SOP's in Fig. 4.3 and find that both SOPs simultaneously vanish at $\delta = 0$. The QPT at $\delta = 0$ corresponds to the continuous change of SOPs from zero to the finite values on either side of the critical point. Similarly we can obtain the odd and even SOPs (O_o^y and O_e^y) in the form similar to Eqs.(4.16).

By looking at Eqs. (4.15) and (4.13), and Fig. 4.3 we note that the even and odd SOPs (O_e^x and O_o^x) are mutually exclusive. A similar conclusion was already presented in the literature [65].

Now we will shortly discuss the local long range order (LRO) defined by $m_x = \langle \sigma_l^x \sigma_m^x \rangle$ in the dimerized XY chain. The LRO parameter derived from the two-spin correlation function in any phase can be expressed as a product of the even and odd

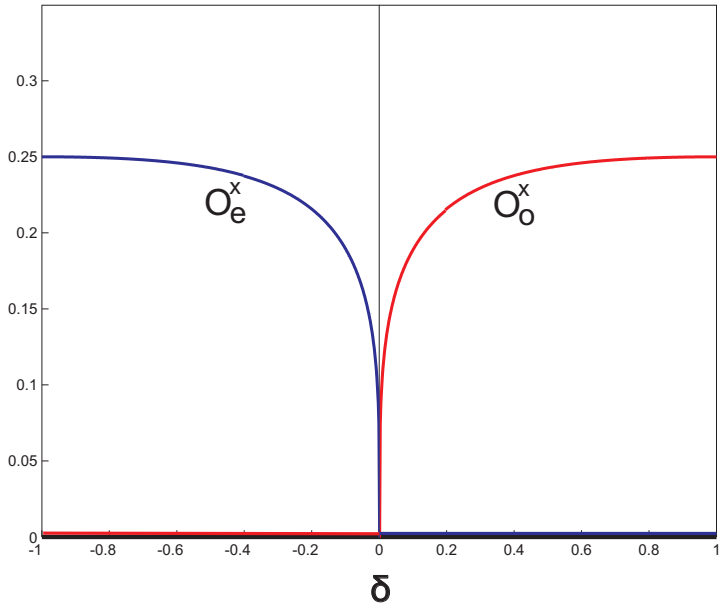

Figure 4.3: SOPs for dimerized XY chain.

SOPs in that phase [see Eqs.(4.31), (4.30), and (4.31) below]

$$m_x = \lim_{l\to\infty} \langle \sigma_1^x \sigma_{2l}^x \rangle \mid_{\delta \leqslant 0} = O_e^x \mid_{\delta \leqslant 0} O_o^x \mid_{\delta \leqslant 0} \tag{4.17}$$

Equation (4.17) indicates that the LRO vanishes in either phases $\delta < 0$ or $\delta > 0$, because one of the two SOPs is always zero(i.e., they are mutually exclusive). Both SOPs are zero in the gapless chain $\delta = 0$. Thus we recover the well-known result that no local long range order is present in the dimerized XY chain.

Let us now discuss the critical behaviour of this spin chain near the critical point. From Eq. (4.16) we can write

$$O_e^x = O_o^x \sim \delta^{2\beta}. \tag{4.18}$$

Hida [63] was the first to point out such critical behaviour of the SOP in the dimer-

ized chain. We find that $\beta = 1/8$ is the critical exponent of order parameter as in the 2D Ising model. As we expressed before, the second critical index $\beta = 1/8$, which proves that the dimerized XY spin chain lies in the same universality class as the 2D Ising model.

4.2 SOP in Anisotropic Dimerized XY chain

To further analyze the correlation functions and topological order in spin models, we choose now the anisotropic dimerized XY spin-1/2. We analyzed this model in chapter 2, and the Hamiltonian (2.1) without magnetic field is written as

$$H = \frac{J}{4}\sum_{i=1}^{N}\left[(1+\gamma)\sigma_i^x\sigma_{i+1}^x + (1-\gamma)\sigma_i^y\sigma_{i+1}^y + \delta(-1)^i\left(\sigma_i^x\sigma_{i+1}^x + \sigma_i^y\sigma_{i+1}^y\right)\right] \qquad (4.19)$$

where J is the exchange coupling of nearest neighbour spin interaction, and γ and δ are the parameters characterizing the degree of anisotropy and dimerization.

This exactly solvable model was proposed by Ye Fei, *et al* [66], and its detailed study can be found in [41]. In this paper [41] they found four branches of the energy spectrum (2.26) by using the JWT. The details on this model are given in chapter 2. The spectrum (2.26) has the energy gap

$$\Delta = J|\delta \pm \gamma| \qquad (4.20)$$

at $k = \pi/2$, and the model is gapless (massless) at $\delta = \pm\gamma$. An illustration of the critical behaviour of the model is shown in Fig. 4.5. The critical lines $\delta = \pm\gamma$ on (γ, δ) plane separates massive phases.

The first two terms in the Hamiltonian (4.19) correspond to the anisotropic XY

model, which was proposed and studied by Lieb and *et al* [67]. They found its energy spectrum, the phase diagram, and correlation functions. The last two terms in the Hamiltonian is the dimerized part of XY model with the dimerization parameter δ.

We rearrange Eq. (4.19) in the even and odd sites with alternating dimerized factor δ, so the Hamiltonian reads

$$H = \frac{J}{4}\sum_{i=1}^{N/2}\left\{(1+\gamma+\delta)\sigma_{2i}^{x}\sigma_{2i+1}^{x} + (1-\gamma+\delta)\sigma_{2i}^{y}\sigma_{2i+1}^{y}\right\}$$

$$+\frac{J}{4}\sum_{i=1}^{N/2}\left\{(1+\gamma-\delta)\sigma_{2i+1}^{x}\sigma_{2i+2}^{x} + (1-\gamma-\delta)\sigma_{2i+1}^{y}\sigma_{2i+2}^{y}\right\} \tag{4.21}$$

Now we map the σ operators onto the dual τ operators using duality transformation (1.23a) and (1.23b) [29, 68]. Then the Hamiltonian (4.21) reads in the dual (τ) space as:

$$H = \frac{1}{4}\sum_{i=1}^{N/2}\left\{\left(J^{++}\tau_{2i-1}^{x}\tau_{2i+1}^{x} + J^{--}\tau_{2i+1}^{y}\right) + \left(J^{+-}\tau_{2i}^{x}\tau_{2i+2}^{x} + J^{-+}\tau_{2i}^{y}\right)\right\} \tag{4.22}$$

It corresponds to two decoupled 1D Ising models in transverse field for odd and even sites in the dual lattice representation. Here we use the notations

$$J^{\pm\pm} = J(1 \pm \gamma \pm \delta). \tag{4.23}$$

By comparing the Hamiltonians (4.22) and (4.6) one can conclude that the dimerized XY chain and the anisotropic dimerized XY chain can both be mapped onto two 1D QIM on the dual lattice. Now let us analyze the conditions for the even and odd Hamiltonians in Eq. (4.22) to possess LRO in the τ-space. The occurrence of the LRO depends on the factor λ [62, 64] as we discussed above, [see Eqs. (4.9) and

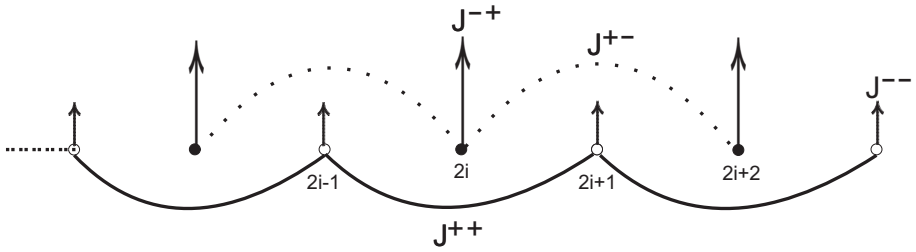

Figure 4.4: Odd and even decoupled Ising chains in transverse field in the dual space. Solid and dotted lines represent the couplings on odd and even sites, respectively.

(4.11)]. The odd dual lattice is ordered when

$$\lambda_o^x = \frac{J^{++}}{J^{--}} = \frac{1+\gamma+\delta}{1-\gamma-\delta} > 1, \tag{4.24}$$

and the LRO is signalled by the non-vanishing correlation function $\langle \tau_1^x \tau_{2i+1}^x \rangle$ (see Eq. 4.9). The system is ordered in the region $\delta > -\gamma$ of the (δ, γ) plane and disordered otherwise as shown in Fig. 4.5. Thus $\langle \tau_{2i+1}^x \rangle$ is an order parameter describing the phase transition when δ crosses from $\delta > -\gamma$ to $\delta \leq -\gamma$. The odd string order parameter defined by Eq. (1.34) for the odd sites, is found as:

$$O_o^x = \begin{cases} \frac{1}{4}\left[\frac{4(\gamma+\delta)}{(1+\gamma+\delta)^2}\right]^{\frac{1}{4}} & \delta > -\gamma \\ 0 & \delta \leq -\gamma \end{cases} \tag{4.25}$$

Similarly, the LRO detected by non-vanishing limit of the correlation function $\langle \tau_2^x \tau_{2i+2}^x \rangle$ defined on the even lattice sites, exists under the following condition:

$$\lambda_e^x \equiv \frac{J^{+-}}{J^{-+}} = \frac{1+\gamma-\delta}{1-\gamma+\delta} > 1. \tag{4.26}$$

The even 1D QIM becomes ordered in the region $\delta < \gamma$ separated by the critical line $\delta = \gamma$ in the (δ, γ) plane and disordered in the $\delta > \gamma$ region. So $\langle \tau_{2i}^x \rangle$ is an order

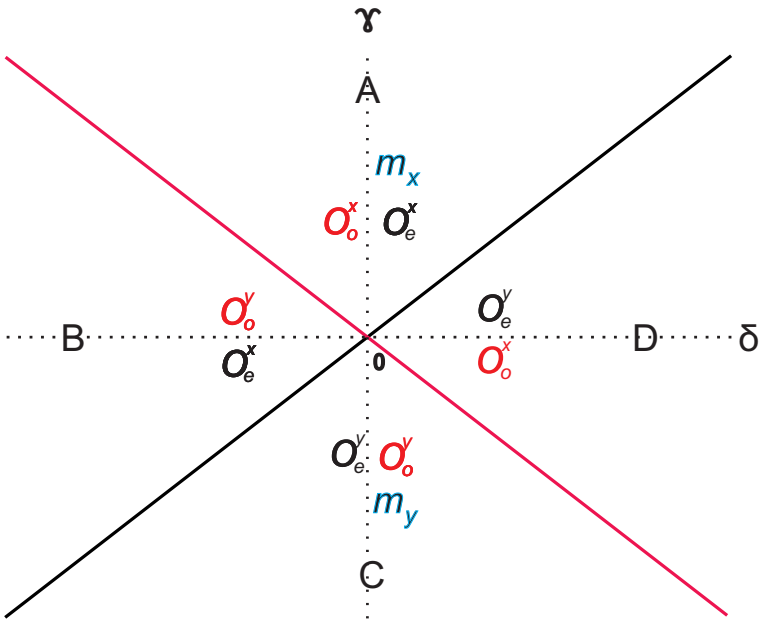

Figure 4.5: Nonvanishing SOPs and local order parameters of the anisotropic dimerized XY chain in the four sectors A,B,C,D of the (δ, γ) parametric plane. The black/red lines $\gamma = \pm\delta$ are the lines of quantum criticality where the model is gapless.

parameter characterizing the phase transition at $\delta = \gamma$. Using the even part of the Hamiltonian (4.22) and Eq. (1.34) we find the even string order parameter

$$O_e^x = \begin{cases} \frac{1}{4}\left[\frac{4(\gamma-\delta)}{(1+\gamma-\delta)^2}\right]^{\frac{1}{4}} & \delta < \gamma \\ 0 & \delta \geq \gamma \end{cases} \tag{4.27}$$

The original Hamiltonian (4.19) is not symmetric with respect to x and y spin components due to the anisotropy parameter γ. So it is natural to also analyze the y component of the even and odd string order parameters. The easiest way to do it is to swap x and y components in the dual transformation (1.23a) and (1.23b). This results in the Hamiltonian (4.22) where x and y components of τ spins are interchanged. Following the lines of above derivations we find two y-components of

SOP:

$$O_o^y = \begin{cases} \frac{1}{4}\left[\frac{-4(\gamma+\delta)}{(1-\gamma-\delta)^2}\right]^{\frac{1}{4}} & \delta < -\gamma \\ 0 & \delta \geq -\gamma \end{cases} \tag{4.28}$$

and

$$O_e^y = \begin{cases} \frac{1}{4}\left[\frac{4(\gamma-\delta)}{(1-\gamma+\delta)^2}\right]^{\frac{1}{4}} & \delta > \gamma \\ 0 & \delta \leq \gamma \end{cases} \tag{4.29}$$

In Fig. 4.5 we show four regions (A,B,C,D) separated by the phase boundaries $\gamma = \pm\delta$. In each region we indicate non-vanishing SOPs (O_o^x, O_e^x, O_o^y and O_e^y). One can infer from Eqs. (4.25),(4.27),(4.28), (4.29) and Fig. 4.5 that a pair of SOP, i.e., $O_\sharp^x$ or $O_\sharp^y$ ($\sharp = e, o$) are mutually exclusive to the regions (B, D), while they co-exist in the regions (A,C). We will show in the next section that coexisting SOPs (O_e^x, O_o^x) and (O_e^y, O_o^y) result in a non-vanishing conventional (local) LRO. The values of the SOPs are given by Eqs. (4.25), (4.27), (4.28) and (4.29).

4.2.1 Correlation Functions and Local LRO

To test a possibility of a local LRO we are going to calculate the limits of correlation functions at large distance. The magnetisation m_x is defined via the correlation function $\langle\sigma_1^x\sigma_{2l}^x\rangle$ as

$$m_x^2 = \lim_{l\to\infty}\langle\sigma_1^x\sigma_{2l}^x\rangle = \lim_{l\to\infty}\langle(\tau_0^x\tau_{2l}^x)(\tau_1^x\tau_{2l-1}^x)\rangle, \tag{4.30}$$

where the last equality follows from the duality transformation (1.23a). The duality transformation of the original Hamiltonain (4.21) maps it onto two decoupled (odd and even) 1D QIM (4.22) on the dual lattice. This means the statistical average of the product of non interacting even and odd τ spins decouples, i.e., $\langle OO'\rangle = \langle O\rangle\langle O'\rangle$, where O and O' are two independent operators. By using Eqs. (1.34), (4.25) and

(4.27) we obtain an interesting result that the correlation function on the original lattice becomes a product of odd and even SOPs which in turn are given by the local correlation functions on the dual lattice lattice (4.30). Finally we get

$$m_x^2 = 16 O_o^x O_e^x = 2 \frac{(\gamma^2 - \delta^2)^{\frac{1}{4}}}{[(1+\gamma)^2 - \delta^2]^{\frac{1}{2}}} \tag{4.31}$$

This LRO parameter is non zero and changes continuously in the region A ($\gamma > \pm\delta$) in Fig. 4.5 and vanishes at the critical lines $\gamma = \pm\delta$. By setting $\delta = 0$ in Eq. (4.31) we obtain the magnetisation given by Eq. (4.1) in Ref. [43] for zero field of the anisotropic XY model. In the similar fashion, we find the magnetisation m_y via the correlation function $\langle \sigma_1^y \sigma_{2l}^y \rangle$ as

$$m_y^2 = \lim_{l \to \infty} \langle \sigma_1^y \sigma_{2l}^y \rangle = 2 \frac{(\gamma^2 - \delta^2)^{\frac{1}{4}}}{[(1-\gamma)^2 - \delta^2]^{\frac{1}{2}}} \tag{4.32}$$

This long range order parameter is non zero and changes continuously in the region C ($\gamma < \pm\delta$) in fig. 4.5 and vanishes at the critical lines $\gamma = \pm\delta$. From Fig. 4.5 we conclude that the string order parameters (SOP) O_o^x, O_e^x and long range order m_x coexist in the region $\gamma > \pm\delta$; and O_o^y, O_e^y and m_y coexist in the region $\gamma < \pm\delta$. The order in the regions B and D in Fig. 4.5 is non local and only contains SOPs: O_o^x, O_e^y and O_e^x, O_o^y, respectively.

In order to study critical properties of the model near the phase boundaries $\gamma = \pm\delta$ we analyze the critical exponents. From Eqs. (4.25), (4.27), (4.28), and (4.29) we write

$$O^x \sim |t|^{2\beta} \tag{4.33}$$

and from Eq. (4.31) and (4.32) we have

$$m_x = \sqrt{O^x} \sim |t|^\beta \tag{4.34}$$

with $|t| \equiv |\delta - \gamma|$. From the above equations and the gap equation (4.20) we can infer that $\beta = 1/8$ and $\nu = 1$. So this exactly solvable model maps onto free fermions also lies in the universality class of the 2D Ising model.

To summarize:

In this chapter we calculate exactly the string order parameter (SOP) and conventional local LRO parameters in the anisotropic dimerized spin-1/2 chain. At first, we used the well-known spin duality transformation [29] to map spin operators from the direct to dual lattice such that the Hamiltonian on the dual lattice becomes that of the two decoupled (odd and even) 1D QIM. Using this transformation we found that the LRO on the dual lattice becomes the SOP on the direct lattice. By using the standard result from Ref. [62, 64] we obtained the LRO parameters on the dual lattice which is the SOP on the direct lattice. Then by using the duality transformation we also found the exact result for the conventional order parameter (magnetisation) via SOPs. We presented the phase diagram in Fig. 4.5 where all nonvanishing local and string order parameters were found.

As a similar special case we also analyzed the dimerized XY chain. We confirmed the well-known result that no local LRO is present in this model. However, the dimerized XY chain possesses the non local string order, and we analytically calculated two SOPs in that model.

Chapter 5

Topological Winding Numbers

In recent years, it has been proven that the phase transitions in spin systems with hidden (nonlocal) orders are accompanied by a change of topological numbers (indices). In this chapter we study the winding number or the Pontryagin index in the spin chains and ladders to understand how it characterizes different gapped phases.

5.1 Winding Number in the Anisotropic Dimerized XY Chain.

To discuss the topological order in the spin system we study the anisotropic dimerized XY spin-1/2 chain (4.19) which was analyzed in chapter 4. We used the 1D JWT to map the spin operators onto the free fermionic operators. To further manipulate the Hamiltonian in the momentum space we use the Fourier transform. By using the Nambu formalism in the odd and even lattice, we find the single particle Hamiltonian (2.21) with the spinor (2.22) and the 4×4 Hamiltonian matrix which

can be worked out in the following way:

$$\mathcal{H}(k) = \begin{pmatrix} 0 & Jc^* & 0 & Ja^* \\ Jc & 0 & Ja^* & 0 \\ 0 & Ja & 0 & -Jc^* \\ Ja & 0 & -Jc & 0 \end{pmatrix}$$

$$= \begin{pmatrix} Jc^{'}\sigma_1 + Jc^{''}\sigma_2 & -iJa\sigma_1 \\ Jia\sigma_1 & -Jc^{'}\sigma_1 - Jc^{''}\sigma_2 \end{pmatrix}$$

$$= Jc^{'} \begin{pmatrix} \sigma_1 & 0 \\ 0 & -\sigma_1 \end{pmatrix} + Jc^{''} \begin{pmatrix} \sigma_2 & 0 \\ 0 & -\sigma_2 \end{pmatrix} + Ja \begin{pmatrix} 0 & -i \\ i & 0 \end{pmatrix}$$

$$= Jc^{'}\sigma_3 \otimes \sigma_1 + Jc^{''}\sigma_3 \otimes \sigma_2 + Ja\sigma_2 \otimes \sigma_1 \tag{5.1}$$

Here we denote $a = i\gamma \sin k$ and $c = c^{'} + ic^{''}$, with $c^{'} = \cos k$ and $c^{''} = \delta \sin k$. σ_α with $\alpha = 1, 2, 3$ are 2×2 Pauli matrices defined by Eq. (1.2). We diagonalize the Hamiltonian matrix (5.1) with the help of Mathematica. The energy spectrum is

$$\pm\epsilon^{\pm}(k) = \pm J\sqrt{\cos^2 k + (\delta \pm \gamma)^2 \sin^2 k} \tag{5.2}$$

in the momentum space which is similar to Eq. (2.26). As we discussed before, the model shows quantum critical behaviour at $\delta = \pm\gamma$ on the (δ, γ) plane and the critical lines separate four gapped (massive) phases [41] as shown in Fig. 4.5.

Following [39, 40] and earlier discussions in section 1.5, we introduce the normalized two component vector (n_x, n_y). From Eq. (5.2) we get

$$n_x = \frac{\cos k}{\sqrt{\cos^2 k + (\delta \pm \gamma)^2 \sin^2 k}} \tag{5.3a}$$

and

$$n_y = \frac{(\delta \pm \gamma)\sin k}{\sqrt{\cos^2 k + (\delta \pm \gamma)^2 \sin^2 k}} \tag{5.3b}$$

We differentiate Eqs. (5.3a) and (5.3b) w.r.t k and plug them into Eq. (1.37). We get

$$\begin{aligned} N_\pm &= \frac{1}{2\pi}\int_0^{2\pi} \frac{(\xi_\pm)}{\cos^2 k + (\xi_\pm)^2 \sin^2 k} \\ &= \frac{2\xi_\pm}{\pi i(1-(\xi_\pm)^2)} \oint_c \frac{z dz}{(z^2 + \frac{1-\xi_\pm}{1+\xi_\pm})(z^2 + \frac{1+\xi_\pm}{1-\xi_\pm})} \end{aligned} \tag{5.4}$$

where we changed the variable k into the complex plane by using $z = e^{ik}$, and the limit of integration from $(-\pi, \pi)$ to $(0, 2\pi)$ because it is symmetrical in this range. Eq. (5.4) has four poles on the imaginary axis. They are; $z_{1,2} = \pm i\sqrt{(1-\xi_\pm)/(1+\xi_\pm)}$, $z_3 = -1/z_1$ and $z_4 = -1/z_2$, with $\xi_\pm = (\delta \pm \gamma)$.

To find the winding number the positions of poles are to be identified in that plane. In addition we have to figure out a pair of the eigenvalues that provides the minimum energy gap and it vanishes at the critical line. From the analysis of the eigenvalues (5.2) we can show that the winding number in any region of the (δ, γ) plane is defined as follows:

$$N_w = \begin{cases} N_+ & \text{if } \ |\xi_+| > |\xi_-| \Leftrightarrow \epsilon^+_{min}(k) < \epsilon^-_{min}(k); k \in [0, \pi] \\ N_- & \text{if } \ |\xi_+| < |\xi_-| \Leftrightarrow \epsilon^-_{min}(k) < \epsilon^+_{min}(k); k \in [0, \pi] \end{cases} \tag{5.5}$$

At first we find N_+ and N_- in all regions $(A', A'', B, C, D', D'', E, F)$ as shown in Fig. 5.2 and then check which pair of eigenvalues (5.2) provides the minimum energy gap [see Fig. 5.1].

(1) For $\delta > \gamma$ regions: (E, F, A', A'')

In these regions we find the term $\xi_- = \delta - \gamma > 0$ and two poles $z_1 = i\sqrt{(1-\xi_-)/(1+\xi_-)} <$

i and $z_2 = -i\sqrt{(1-\xi_-)/(1+\xi_-)} > -i$ lie inside the circle of unit radius. We find two residues at poles z_1 and z_2 and their sum is

$$a_{-1}|_{z\to z_1} + a_{-2}|_{z\to z_2} = \lim_{z\to z_1} \frac{z}{(z-z_2)(z-z_3)(z-z_4)}$$

$$+ \lim_{z\to z_2} \frac{z}{(z-z_1)(z-z_3)(z-z_4)}$$

$$= \frac{1-\xi_-^2}{4\xi_-} \tag{5.6}$$

Using the residue theorem; $\oint_c f(z)dz = 2\pi i \sum_i a_{-1}|_{z=z_i}$ and Eq. (5.6) in Eq. (5.4),the winding number becomes

$$N_- = 1 \tag{5.7}$$

(2) For $\delta < \gamma$ regions: (B, C, D', D'')

In these regions we find the quantity $\xi_- = \delta - \gamma < 0$ and two poles $z_3 = i\sqrt{(1+\xi_-)/(1-\xi_-)} < i$ and $z_4 = -i\sqrt{(1+\xi_-)/(1-\xi_-)} > -i$ lie inside the circle of unit radius. The sum of residues at these two poles is

$$a_{-1}|_{z\to z_3} + a_{-1}|_{z\to z_4} = \lim_{z\to z_3} \frac{z}{(z-z_1)(z-z_2)(z-z_4)}$$

$$+ \lim_{z\to z_4} \frac{z}{(z-z_1)(z-z_2)(z-z_3)}$$

$$= -\frac{1-\xi_-^2}{4\xi_-} \tag{5.8}$$

By using the residue theorem; $\oint_c f(z)dz = 2\pi i \sum_i a_{-1}|_{z=z_i}$ and Eq. (5.8) in Eq. (5.4) we obtain

$$N_- = -1 \tag{5.9}$$

Similarly, we calculate the winding number N_+ in $\delta > -\gamma$ regions (A', A'', B, C) and

in $\delta < -\gamma$ regions (D', D'', E, F). It takes two values; $N_+ = 1$ and $N_+ = -1$ in the above mentioned respective regions on the (δ, γ) plane.

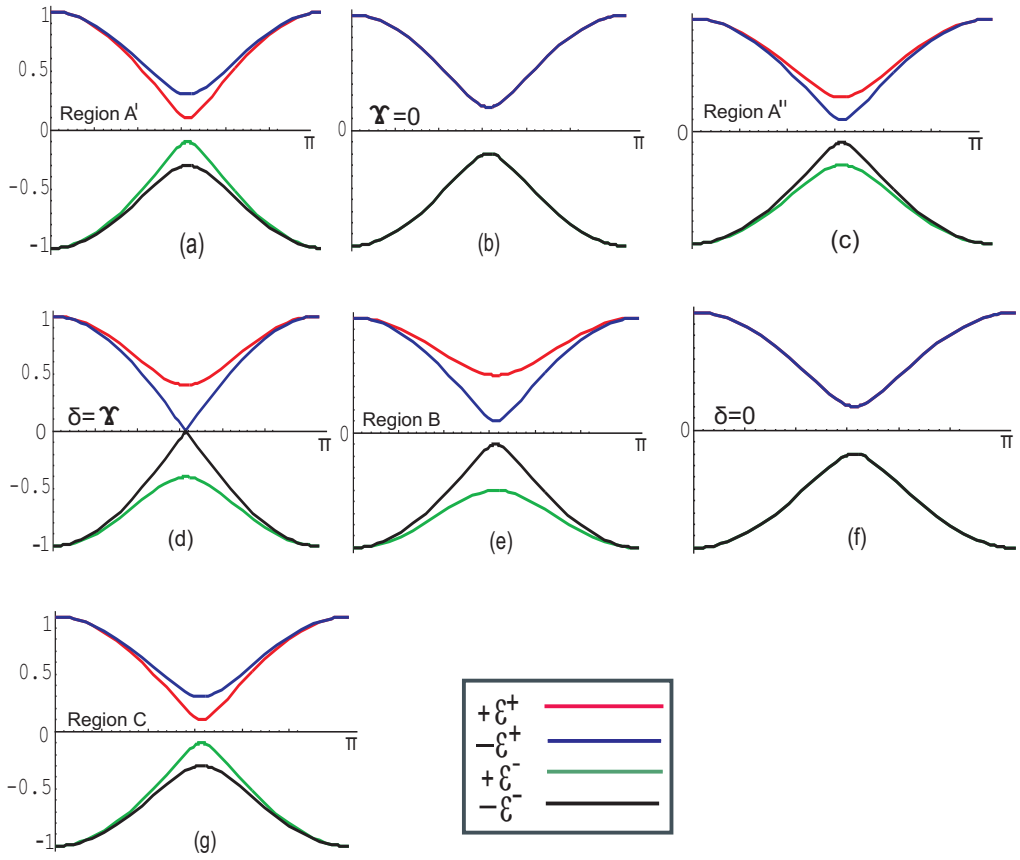

Figure 5.1: The four energy eigenvalue spectrum of a chain in different regions of the parametric plane (a) $\delta = 0.25$, $\gamma = -0.1$; (b) $\delta = 0.2$, $\gamma = 0$; (c) $\delta = 0.2$, $\gamma = 0.1$; (d) $\delta = 0.2$, $\gamma = 0.2$; (e) $\delta = 0.2$, $\gamma = 0.3$: (f) $\delta = 0$, $\gamma = 0.2$, and (g) $\delta = -0.2, \gamma = 0.3$. The vertical axis is the energy and the horizontal axis is the angle in the k space taken from 0 to π.

In order to understand why the winding number changes the sign while crossing the line at $\delta = 0$ and $\gamma = 0$, we plot energy eigenvalues in the regions (A', A'', B, C). The curves shown in Figs. 5.1a, 5.1b, and 5.1c are in region A', on line at $\gamma = 0$, and region A'', respectively. In the figures the two pairs of eigenvalues cross the energy levels while crossing the line at $\gamma = 0$. As we can see from (5.3a), (5.3b),

and (5.5) the winding number changes the unit vector which is used to calculate N_w when the line $\gamma = 0$ is crossed. A similar phenomenon appears in the Figs. 5.1e, 5.1f, 5.1g. Now we can infer that the change of the winding number is not necessarily accompanied by the gap closing or any type of phase transitions. This change of topological index is associated with the level crossing only. From Figs. 5.1c, 5.1d, 5.1e we see that the winding number changes the sign while crossing the phase boundary $\delta = \gamma$. The change of the winding number at the critical line, where the gap closes, signals the real topological phase transition. Similar physical phenomenon appear in the regions (D',D'',E,F) and winding numbers in all regions are shown in the Fig. 5.2

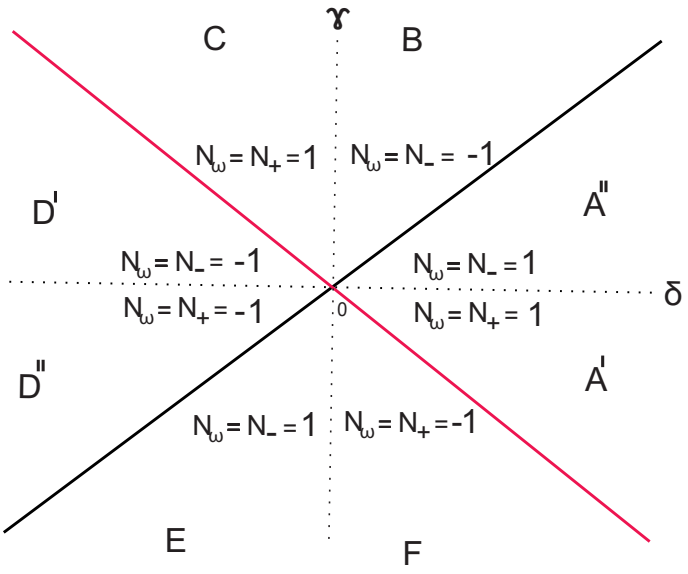

Figure 5.2: Winding numbers on the parametric $(\gamma - \delta)$ plane of the anisotropic dimerized XY chain.

5.2 Winding Number in Dimerized Ladders

In order to further analyze the unconventional gapped phases in the dimerized Heisenberg two-leg spin ladder we calculate its topological winding number. We

have studied two possible dimerizations in this ladder in chapter 3. In this section we use the approximate free-fermionic Hamiltonians derived for the two dimerization patterns in the previous chapter to calculate the topological Pontryagin indices for the different massive phases in the two-leg ladder.

5.2.1 Staggered Phase.

The structure and basic properties of two-leg spin ladder in the case of alternated dimerization pattern were studied in chapter 3. Now we can use those results here. In the framework of Hartree-Fock approximation we found the free-fermionic effective Hamiltonian (2.21) with 4×4 Bloch Hamiltonian matrix which we rewrite here in a more compact form:

$$\mathcal{H} = \begin{pmatrix} 0 & -J_R c & \frac{1}{2}J_{\perp R} & 0 \\ -J_R c^* & 0 & 0 & \frac{1}{2}J_{\perp R} \\ \frac{1}{2}J_{\perp R} & 0 & 0 & -J_R c^* \\ 0 & \frac{1}{2}J_{\perp R} & -J_R c & 0 \end{pmatrix}$$

$$= \begin{pmatrix} -J_R(c^{'}\sigma_1 - c^{''}\sigma_2) & \frac{1}{2}J_{\perp R}\mathbb{1} \\ \frac{1}{2}J_{\perp R}\mathbb{1} & -J_R(c^{'}\sigma_1 + c^{''}\sigma_2) \end{pmatrix}$$

$$= -J_R c^{'} \begin{pmatrix} \sigma_1 & 0 \\ 0 & \sigma_1 \end{pmatrix} + J_R c^{''} \begin{pmatrix} \sigma_2 & 0 \\ 0 & -\sigma_2 \end{pmatrix} + \frac{1}{2}J_{\perp R} \begin{pmatrix} 0 & \mathbb{1} \\ \mathbb{1} & 0 \end{pmatrix}$$

$$= -J_R c^{'} \mathbb{1} \otimes \sigma_1 + J_R c^{''} \sigma_3 \otimes \sigma_2 + \frac{1}{2}J_{\perp R}\sigma_1 \otimes \mathbb{1} \tag{5.10}$$

where $\sigma_{1,2,3}$ are Pauli matrices. For simplicity we denote $c = c^{'} + ic^{''}$ with $c^{'} = \delta \cos k$ and $c^{''} = \sin k$. The sign $\otimes$ used in Eq. (5.10) is the tensor product of matrices. We can now use the gamma matrices defined by (1.4) in the Hamiltonian (5.10). We

get

$$\mathcal{H} = \left(J_R \delta \cos k \pm \frac{J_{R\perp}}{2} \right) \Gamma_1 + (J_R \sin k)\Gamma_4 \equiv d_1^{\pm}\Gamma_1 + d_4\Gamma_4 \tag{5.11}$$

We diagonalize the Hamiltonian (5.11) by using Mathematica and find the four eigenvalues $\pm\sqrt{d_1^2 + d_4^2}$ by Eq. (3.25). The Hamiltonian (3.17) has the diagonal form

$$H = \sum_{\nu=1}^{4} \int_0^{\pi} \epsilon_\nu(k)\eta_\nu^\dagger(k)\eta_\nu(k)dk \tag{5.12}$$

where $\epsilon_\nu(\nu = 1, 2, 3, 4)$ are compact notations for $\epsilon^+, \epsilon^-, -\epsilon^+, -\epsilon^-$ respectively [see Eq. (3.25)]. These eigenvalues are shown in Fig. 5.3, where a couple of eigenvalues are related by a shift $\epsilon_1(k) \equiv \epsilon_2(\pi + k)$.

Let us take two positive eigenvalues first $(\nu = 1, 2)$ in Eq. (5.12), so

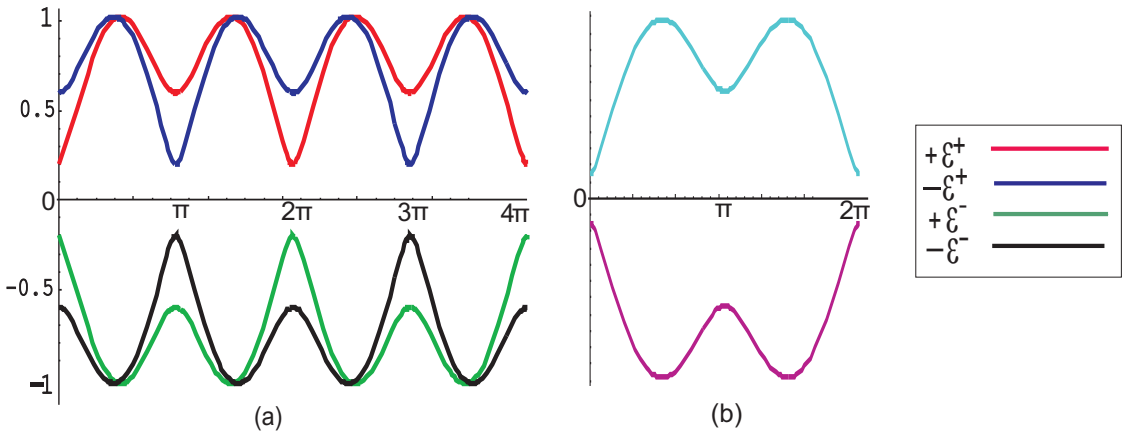

Figure 5.3: (a) Four energy eigenvalues of staggered ladder at model's parameters $\delta = 0.25, J_\perp/2J = 0.4$ (b) Integration with the branch ϵ_1 in the region $[0, \pi]$ and with the branch ϵ_2 in the region $[\pi, 2\pi]$ is mapped on a single branch in the region $[0, 2\pi]$ (sky blue). Similar mapping of the negative branches (magenta).

$$H_1 + H_2 = \int_0^{\pi} \epsilon_1(k)\eta_1^\dagger(k)\eta_1(k)dk + \int_0^{\pi} \epsilon_2(k)\eta_2^\dagger(k)\eta_2(k)dk$$

$$= \int_0^{2\pi} \epsilon_2(k)\widetilde{\eta}_2^\dagger(k)\widetilde{\eta}_2(k)dk \tag{5.13}$$

where we used the relation $\epsilon_1(k) = \epsilon_2(\pi + k)$ and we defined new operators

$$\widetilde{\eta}_2(k) = \begin{cases} \eta_2(k) & k \in [0, \pi] \\ \eta_1(k - \pi) & k \in [\pi, 2\pi] \end{cases} \tag{5.14}$$

Similarly, the last two terms in the Hamiltonian (5.12) for the negative energies can be brought into the following form:

$$H_3 + H_4 = \int_0^{2\pi} \epsilon_4(k)\widetilde{\eta}_4^\dagger(k)\widetilde{\eta}_4(k)dk \tag{5.15}$$

Then Eqs. (5.13) and (5.15) yield

$$H = \sum_{\nu=\pm} \nu \int_0^{2\pi} \epsilon(k)\widetilde{\eta}_\nu^\dagger(k)\widetilde{\eta}_\nu(k)dk \tag{5.16}$$

with eigenvalues

$$\pm\epsilon(k) = \pm\sqrt{(J_R \sin k)^2 + \left(J_R\delta\cos k - \frac{J_{\perp R}}{2}\right)^2} \tag{5.17}$$

Now we introduce the normalized vector $(n_x, n_y) = (d_1^-, d_4)/|d|$ where

$$n_x(k) = \frac{J_R\delta\cos k - J_{\perp R}/2}{\sqrt{(J_R \sin k)^2 + \left(J_R\delta\cos k - \frac{J_{\perp R}}{2}\right)^2}} \tag{5.18a}$$

and

$$n_y(k) = \frac{J_R \sin k}{\sqrt{(J_R \sin k)^2 + \left(J_R\delta\cos k - \frac{J_{\perp R}}{2}\right)^2}} \tag{5.18b}$$

We differentiate Eqs. (5.18a) and (5.18b) and plug them in Eq. (1.37). The winding

number becomes

$$N_w = \frac{J_R}{2\pi} \oint_c \frac{(J_R\delta - \frac{J_{\perp R}}{2}\cos k)}{(J_R \sin k)^2 + \left(J_R\delta\cos k - \frac{J_{\perp R}}{2}\right)^2} dk \tag{5.19}$$

To simplify Eq. (5.19) we change the variable in the complex plane by using the relation $z = e^{ik}$ and introduce the notations: $2J_1 = J_R(1+\delta)$, $2J_2 = -J_R(1-\delta)$, $2J_3 = J_{\perp R}$, $J_+ = J_1 + J_2 = J_R\delta$ and $J_- = J_1 - J_2 = J_R$. It yields

$$N_w = \frac{J_-}{4\pi i} \oint_c \frac{J_3 z^2 + 2zJ_+ + J_3}{(J_1 z^2 + zJ_3 + J_2)(J_2 z^2 + zJ_3 + J_1)} dk \tag{5.20}$$

The integrand in Eq. (5.20) has four poles on the real axis. They are

$$z_{1,2} = \frac{1}{1+\delta}\left[-\left(\frac{J_{\perp R}}{2J_R}\right) \pm \sqrt{\left(\frac{J_{\perp R}}{2J_R}\right)^2 + (1-\delta^2)}\right], \tag{5.21}$$

In the Fig. 5.4 we show the four regions (A,B,C,D) separated by the phase boundaries $\delta = \pm J_{\perp R}/2J_R$ in the parametric plane $(\delta, J_\perp/2J)$. These boundaries were previously found from Eq. (3.26). Now we can study N_w in four gapped phases.

Phase A:

In this phase we find $\delta > 0$ and $\delta > \pm J_{\perp R}/2J_R$, then $\frac{1-\delta}{1+\delta} < z_1 \leq 1$; $-1 \leq z_2 < \frac{\delta-1}{1+\delta}$; $z_3 \geq 1$ and $z_4 \leq -1$. The two poles z_1 and z_2 lie inside the circle of unit radius. The residues at z_1 and z_2 are

$$a_{-1}|_{z=z_1} = \lim_{z\to z_1}(z-z_1)\frac{(J_3 z^2 + 2J + z + J_3)}{(z-z_1)(z-z_2)(z-z_3)(z-z_4)}$$

$$= \frac{J_R(1-\delta^2)}{4X}\left[\frac{\frac{J_{\perp R}}{2J_R}\left(X - \frac{J_{\perp R}}{2J_R}\right)^2 + 2\left(X - \frac{J_{\perp R}}{2J_R}\right)(1+\delta)\delta + \frac{J_{\perp R}}{2J_R}(1+\delta)^2}{\left(X - \frac{J_{\perp R}}{2J_R}\right)^2 - (1+\delta)^2}\right] \tag{5.22a}$$

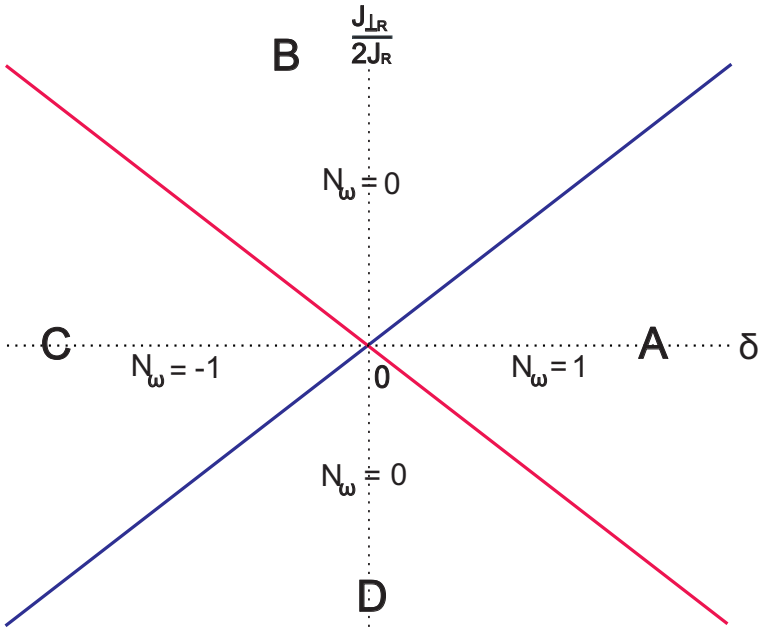

Figure 5.4: The winding number N_w in the phases A,B,C, and D in parametric space $(J_{\perp R}/2J_R, \delta)$ of the staggered phase.

and

$$a_{-1}|_{z=z_2} = -\frac{J_R(1-\delta^2)}{4X}\left[\frac{\frac{J_{\perp R}}{2J_R}\left(X+\frac{J_{\perp R}}{2J_R}\right)^2 - 2\left(X+\frac{J_{\perp R}}{2J_R}\right)(1+\delta)\delta + \frac{J_{\perp R}}{2J_R}(1+\delta)^2}{\left(X+\frac{J_{\perp R}}{2J_R}\right)^2 - (1+\delta)^2}\right] \tag{5.22b}$$

with $X = \sqrt{\left(\frac{J_{\perp R}}{2J_R}\right)^2 + (1-\delta)^2}$. The sum of these residues is

$$a_{-1}|_{z=z_1} + a_{-1}|_{z=z_2} = -\frac{J_R}{2}(1-\delta)^2 \tag{5.23}$$

Now we use the residue theorem; $\oint_c f(z)dz = 2\pi i \sum_i a_{-1}|_{z=z_i}$ and Eq. 5.23), in Eq. (5.20),to obtain

$$N_w = 1 \tag{5.24}$$

Phase B:

In this phase we note that $J_{\perp R}/2J_R > 0$ and $J_{\perp R}/2J_R > \pm\delta$, then $\frac{(1-J_{\perp R}/2J_R)}{(1+J_{\perp R}/2J_R)} < z_1 \leq 1$; $z_2 \geq 1$; $z_3 \leq -1$ and $-1 \leq z_1 < -\frac{(1-J_{\perp R}/2J_R)}{(1+J_{\perp R}/2J_R)}$. The poles z_1 and z_4 lie within the circle of unit radius. The residue at z_4 is,

$$a_{-1}|_{z=z_4} = \frac{J_R(1-\delta^2)}{4X}\left[\frac{\frac{J_{\perp R}}{2J_R}\left(X+\frac{J_{\perp R}}{2J_R}\right)^2 - 2\left(X+\frac{J_{\perp R}}{2J_R}\right)(1+\delta)\delta + \frac{J_{\perp R}}{2J_R}(1+\delta)^2}{\left(X+\frac{J_{\perp R}}{2J_R}\right)^2 - (1+\delta)^2}\right] \tag{5.25}$$

with $X = \sqrt{\left(\frac{J_{\perp R}}{2J_R}\right)^2 + (1-\delta)^2}$. The sum of the residues at z_1 and z_4 becomes

$$a_{-1}|_{z=z_1} + a_{-1}|_{z=z_4} = 0 \tag{5.26}$$

By applying the residue theorem; $\oint_c f(z)dz = 2\pi i \sum_i a_{-1}|_{z=z_i}$ and using Eq. (5.26), Eq. (5.20) reads

$$N_w = 0 \tag{5.27}$$

Similarly, the quantity in Eq. (5.20) takes the values; $N_w = -1$ and $N_w = 0$ in the phases C and D, respectively: [See Fig. 5.4]. In Fig. 5.4 we see that the phases (A,B,C,D) are characterized by the winding numbers $N_w = (1, 0, -1, 0)$, respectively. Using the results shown in the first quadrant in Fig. 5.4 we combine them with the results for the SOPs found in the earlier work [45, 36]. In Fig. 5.5 we show two gapped phases in the positive $(\delta, J_\perp/2J)$ plane, separated by the phase boundary that is represented by a solid line. We indicate winding number that takes the values 1 and 0 in the leg-dimer and rung-dimer phases, respectively. Thus in addition to the SOPs the winding number can be used to characterize the topological phases of the staggered ladder. In this model the topological number can not change its value without crossing the phase boundary.

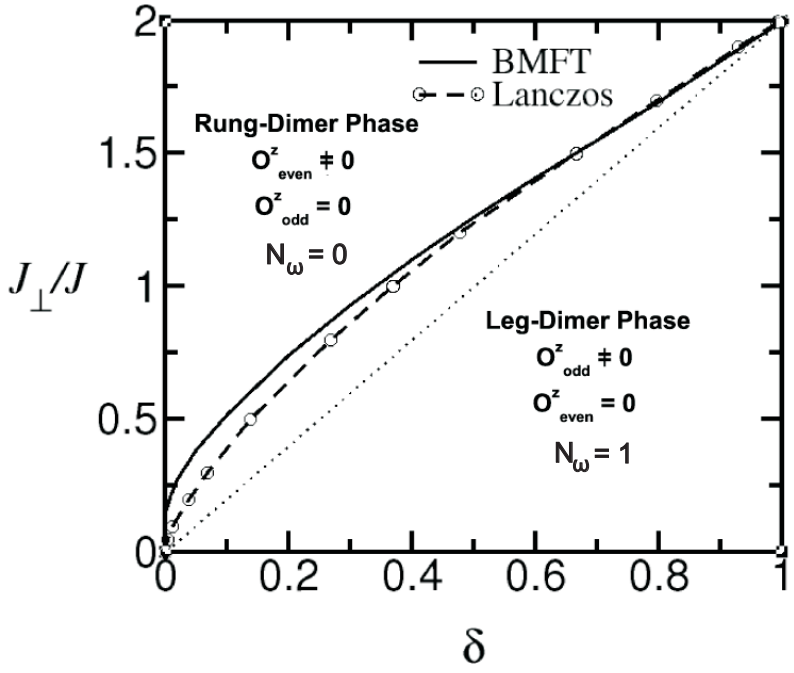

Figure 5.5: Staggered phase of two-leg ladder; critical line $J_{\perp c}(\delta)$ where the gap vanishes. Adapted from Ref.[36] and original data taken from Ref. [55]. In addition to two different SOPs, the two phases of the staggered dimerized ladder are characterized by distinct topological numbers.

5.2.2 Columnar Phase.

We previously found the approximate single-particle fermionic Hamiltonian for this phase. The 4×4 Hamiltonian matrix (3.46) can be written as

$$\mathcal{H} = \begin{pmatrix} 0 & J_R c^* & \frac{1}{2}J_{\perp R} & 0 \\ J_R c & 0 & 0 & \frac{1}{2}J_{\perp R} \\ \frac{1}{2}J_{\perp R} & 0 & 0 & -J_R c^* \\ 0 & \frac{1}{2}J_{\perp R} & -J_R c & 0 \end{pmatrix}$$

$$= \begin{pmatrix} J_R(c^{'}\sigma_1 + c^{''}\sigma_2) & \frac{1}{2}J_{\perp R}\mathbb{1} \\ \frac{1}{2}J_{\perp R}\mathbb{1} & -J_R(c^{'}\sigma_1 + c^{''}\sigma_2) \end{pmatrix}$$

$$= J_R c^{'} \begin{pmatrix} \sigma_1 & 0 \\ 0 & -\sigma_1 \end{pmatrix} + J_R c^{''} \begin{pmatrix} \sigma_2 & 0 \\ 0 & -\sigma_2 \end{pmatrix} + \frac{1}{2} J_{\perp R} \begin{pmatrix} 0 & \mathbb{1} \\ \mathbb{1} & 0 \end{pmatrix}$$

$$= J_R c^{'} \sigma_3 \otimes \sigma_1 + J_R c^{''} \sigma_3 \otimes \sigma_2 + \frac{1}{2} J_{\perp R} \sigma_1 \otimes \mathbb{1} \tag{5.28}$$

Here we denote; $c = c^{'} + ic^{''}$ with $c^{'} = \delta \cos k$ and $c^{''} = \sin k$. We use the gamma matrices (1.4) in the Hamiltonian (5.28) to obtain

$$\mathcal{H} = (J_R \delta \cos k)\, \Gamma_3 + (J_R \sin k)\, \Gamma_4 + \left(\frac{J_{R\perp}}{2}\right) \Gamma_1$$

$$\equiv d_3 \Gamma_3 + d_4 \Gamma_4 + d_1 \Gamma_1 \tag{5.29}$$

We diagonalize the Hamiltonian (5.29) by using Mathematica to find the following energy spectrum (3.47):

$$\pm \epsilon^{\pm}(k) = \pm \sqrt{d_1^2 + d_3^2 + d_4^2}$$

$$= \pm \sqrt{J^2 \sin^2 k + J^2 \delta^2 \cos^2 k + \left(\frac{J_\perp}{2}\right)^2} \tag{5.30}$$

The Hamiltonian (3.45) is always gapped and has the diagonal form

$$H = \int_0^\pi \epsilon^{\pm}(k) \eta^\dagger(k) \eta(k) dk \tag{5.31}$$

From the spectrum (5.30) we write the components of thenormalized vector (d_1, d_3, d_4):

$$n_x(k) = \frac{\delta \cos k}{\sqrt{\sin^2 k + \delta^2 \cos^2 k + \left(\frac{J_\perp}{2J}\right)^2}} \tag{5.32a}$$

$$n_y(k) = \frac{\sin k}{\sqrt{\sin^2 k + \delta^2 \cos^2 k + \left(\frac{J_\perp}{2J}\right)^2}} \tag{5.32b}$$

$$n_z(k) = \frac{J_\perp/2J}{\sqrt{\sin^2 k + \delta^2 \cos^2 k + \left(\frac{J_\perp}{2J}\right)^2}} \tag{5.32c}$$

We differentiate Eqs. (5.32a) and (5.32b) w.r.t k and plug them into Eq. (1.37). The winding number becomes

$$N_w = \frac{1}{2\pi} \int_0^{2\pi} \frac{\delta}{\sin^2 k + \delta^2 \cos^2 k + \left(\frac{J_\perp}{2J}\right)^2} \tag{5.33}$$

where we changed the limit of integration from [-π, π] to $[0, 2\pi]$ by using the symmetry. In order to simplify the above integral (5.33) we change the variable in the complex plane by using the relation $y = z^2 = e^{2ik}$. It reads

$$N_w = \frac{2\delta}{i\pi(\delta^2 - 1)} \oint \frac{1}{\left[y^2 + 2\frac{\left(\delta^2+1+(J_\perp/J)^2\right)}{(\delta^2-1)} + 1\right]} dy \tag{5.34}$$

The integrand in Eq. (5.34) has two poles in the real axis. They are

$$y_\pm = \frac{1}{\delta^2 - 1} \left[-\left(\delta^2 + 2\left(\frac{J_\perp}{2J}\right)^2 + 1\right) \pm 2\sqrt{\left(\frac{J_\perp}{2J}\right)^2 + 1}\sqrt{\left(\frac{J_\perp}{2J}\right)^2 + \delta^2} \right] \tag{5.35}$$

We note that y_+ lies inside the circle of unit radius for whole parametric space $(\delta, J_\perp/2J)$. The residue at the pole y_+ is

$$\begin{aligned} a_{-1}|_{y\to y_+} &= \lim_{y\to y_+} \frac{(y - y_+)}{(y - y_+)(y - y_-)} = \frac{1}{y_+ - y_-} \\ &= \frac{4}{\delta^2 - 1}\sqrt{\left(\frac{J_\perp}{2J}\right)^2 + 1}\sqrt{\left(\frac{J_\perp}{2J}\right)^2 + \delta^2} \end{aligned} \tag{5.36}$$

Now we apply the residue theorem; $\oint_c f(z)dz = 2\pi i \sum_i a_{-1}|_{z=z_i}$ at Eq. (5.33) and use Eq. (5.36) in Eq. (5.35). It gives

$$N_w = \frac{\delta}{\sqrt{\left(\frac{J_\perp}{2J}\right)^2 + 1}\sqrt{\left(\frac{J_\perp}{2J}\right)^2 + \delta^2}} \tag{5.37}$$

From Eq. (5.37) we find that N_w is symmetric with respect to the sign of $J_\perp/2J$.

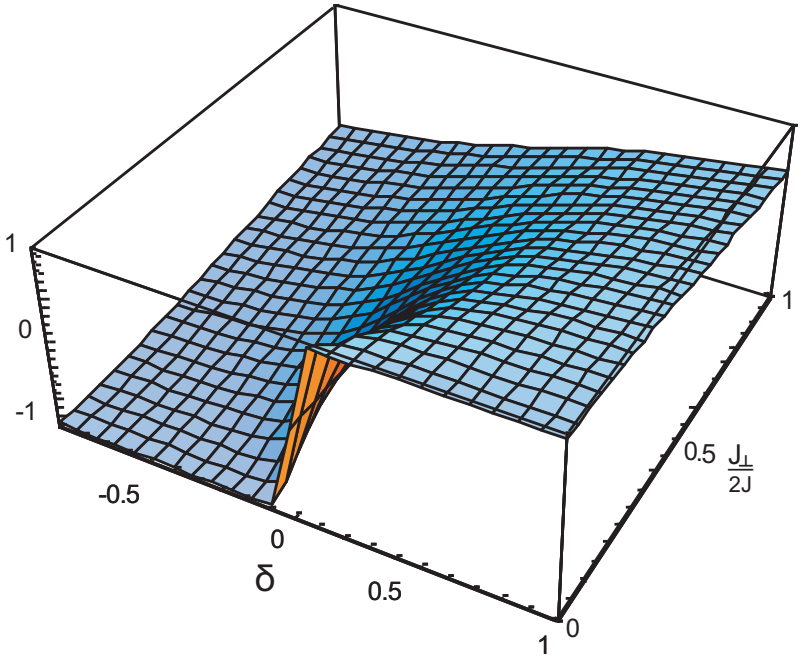

Figure 5.6: The winding number N_w in the $(J_\perp/2J, \delta)$ plane for $J_\perp \geq 0$

So, we plot Fig. 5.6 in $(J_\perp/2J, \delta)$ parameter space only for $J_\perp/2J > 0$. From Fig. 5.6 we can infer that the winding number is no longer quantized to be an integer and it continuously changes from $N_w = 1$ to $N_w = -1$ when we go from $\delta > 0$ to $\delta < 0$ in the whole $(J_\perp/2J, \delta)$ parametric plane. This means that the columnar phase is topologically trivial, as was explained in Ref. [40] for a similar case. This is related to the fact that the mapping of the three-dimensional unit sphere onto a circle is always trivial [40].

On the other hand, in the limit $J_\perp = 0$ (dimerized XY chain) the quantity (5.37) takes

$$N_w = \begin{cases} 1 & \delta > 0 \\ -1 & \delta < 0 \end{cases} \tag{5.38}$$

From Eq. (5.38) we notice that the quantity suddenly changes its integer from 1 to -1 or vice versa at the phase boundary $\delta = 0$. This is an agreement with our earlier results for the anisotropic dimerized chain in the limit $\gamma \to 0$ [see Fig. 5.2].

To summarize:

In this chapter we focused on the study of the winding number (Pontryagin index) to characterize the topological phases of quantum spin systems such as the anisotropic dimerized XY chain and the antiferromagnetic dimerized Heisenberg two-leg spin ladder in two dimerization patterns. The 4×4 single particle Hamiltonians were obtained in terms of the gamma matrices for these models from which the energy spectra were calculated. The winding numbers were calculated analytically by using the residue theorem. We concluded that the winding number characterizes the topological phases by changing the sign while crossing the phase boundaries. The phase transition is also accompanied by emerging nonvanishing SOPs and/or conventional LRO parameters [see Fig. 4.5]. Interestingly, in the anisotropic dimerized XY chain the winding number changes its value in a gapped phase while crossing the line $\delta = 0$ and $\gamma = 0$ without crossing the phase boundary. This change of the topological index is associated to the level crossing only. This exactly solved model provides a counterexample to recent claims in the literature that a change of the topological number signals a topological phase transition without gap closing [40]. In addition, we found that the columnar phase of the ladder is always topologically trivial.

Chapter 6

Conclusions

In the present thesis the quantum phase transitions, non local (topological) and local conventional orders, and the topological numbers in the antiferromagnetic dimerized Heisenberg chains and two-leg ladders were studied. The calculations were carried out for the dimerized XY chain, the anisotropic dimerized XY chain and the two-leg ladder in both the staggered and columnar configurations.

In this work we mapped the spin operators of the original Hamiltonians onto spinless fermionic operators by using the JWT. To treat the ladder we used the MFA for the interacting fermionic terms. Using the Nambu formalism we obtained the single particle 4×4 Hamiltonian matrices for different models and found their eigenvalues.

In both the staggered and the columnar phases of the two-leg ladder quantities such as eigenvalues and energy gap were obtained by using the minimization of the ground state energy. By investigating the mean-field equations in the limit of the model's parameters we confirmed the earlier results [45, 36] that the columnar phase

always remained consistently gapped, whereas the staggered configuration shows the quantum critical behaviour. The quantum phase transition is continuous along the critical line, except in the small region of δ where a small residual gap was detected. We attribute this weak discontinuity of the phase transition to the artefact of the mean-field approximation, since more accurate numerical results clearly indicate a continuous phase transition.

Ultimately the spectra of both the staggered and the columnar configurations of the two-leg ladder were identified with those of the dimerized anisotropic XY spin chains in the transverse magnetic field by comparing the model's parameters. We use these mappings to find more analytical results for the topological phases of the two-leg ladder.

For the first time we calculated the energy spectra and the energy gap in the anisotropic dimerized XY chain in an alternating magnetic field. By investigating the different branches of the eigenvalues we found that the model shows quantum critical behaviour on some critical lines in the (δ, γ) plane. In order to calculate SOPs and local LRO parameters we performed the spin duality transformation and found that the SOPs in the direct lattice were given by the LRO parameters in dual lattice. Moreover, the calculated two pairs (odd, even) of SOPs were mutually exclusive in two phases ($\delta > \pm\gamma$) and ($\delta < \pm\gamma$) and co-existed in the other two phases. We then found the local LRO correlation functions in the phases ($\delta < \pm\gamma$) and ($\delta > \pm\gamma$) by using the SOPs. The same calculations were done in the dimerized XY model and we confirmed the findings that the pair of SOPs are mutually exclusive. A complete phase diagram and the analytical results for the SOPs and local LRO parameters for the whole parameter (δ, γ) plane of the anisotropic dimerized XY chain are presented.

As a complimentary parameter we investigated the topological winding number, or Pontryagin index in $(\delta, \gamma) - XY$ chain and the both configurations of the two-leg antiferromagnetic ladder. These calculations were carried out to further analyze the different topological phases of the models. We found that the different winding numbers characterize the different phases and these topological numbers change their integer values while crossing the phase boundaries. Interestingly, in the $(\delta, \gamma) - XY$ model the winding number changed the sign while crossing the parametric boundaries $\delta = 0$ and $\gamma = 0$ in (δ, γ) plane. This change of winding number is associated with the level crossing of eigenvalues and no phase transition or crossover occurs on those lines $\delta = 0$ and $\gamma = 0$. In addition, in the columnar configuration the winding number changed continuously from one region to the other in the gapped phase. It is topologically trivial.

In future work we will further analyze the analytical results by using the free-fermionic Hamiltonian (3.17) [54]. We also plan to advance further our research for ladders with different numbers of legs and types of interactions, as well as for 2D spin models.

Bibliography

[1] A. Gogolin, A. Nersesyan, and A. Tsvelik, *Bosonization and Strongly Correlated Systems*, Cambridge Press, (1998)

[2] E. Fradkin, *Field theories of condensed matter systems*, Cambridge University Press (second eddition), New York (2013)

[3] E. Dagotto and A. Moreo, Phys. Rev. B **38**, 5087 (1988).

[4] T. Barnes, E. Dagotto, J. Riera and E. S. Swanson, Phys. Rev. B **47**, 3196 (1993).

[5] M.A. Martin-Delgado, J. Dukelsky, and G. Sierra, Phys. Lett. A **250**, 87 (1998).

[6] J. Reger and A. Young, Phys. Rev. B **37**, 5978 (1988).

[7] J. Almeida, M. A. Martin-Delgado and G. Sierra, Phys. Rev. B **76**, 184428 (2007).

[8] E. Dagotto and T. M. Rice, Science **271**, 618 (1996).

[9] M. Kohmoto and H. Tasaki, Phys. Rev. B **46**, 3846 (1992)

[10] E. Lieb and D. Mattis, *Perspectives in Physics: Mathematical Physics in One Dimension*, Academic Press Inc., (1966).

[11] S. Flugge, *Practical Quantum Mechanics II*, Springer-Verlag, Berlin Heidelberg New York, (1971).

[12] J. J. Sakurai, *Advanced Quantum Mechanics*, Addison-Wesley Publishing Company (1967)

[13] M. Fruchart and D. Carpentier, arXiv: 1310.0255v1 (2013)

[14] T. Giamarchi, *Quantum Physics in One Dimension*, International Series of Monographs on Physics, Clarendon Press, Oxford (2004).

[15] J.J. Sakurai, *Modern Quantum Mechanics*, Revised Ed., Addison Wesley, (1994) pp. 362.

[16] H. Bethe, Z. Phys. **71**, 205 (1931).

[17] P. Jordan and E. Wigner, Z. Phys. **47**, 631 (1928).

[18] E. Lieb, T. Schultz, and D. Mattis, Ann. Phys. (N.Y) **16**, 407 (1963).

[19] A. J. Heeger, S. Kivelson, J. B. Schrieffer and W.-P. Su, Rev. Mod. Phys. **60**, 781 (1988).

[20] M. Holicki and H. Fehske, J. Magn. Mater. **22**, 397 (2001).

[21] F. D. M. Haldane, Phys. Lett. **93A**, 464 (1983).

[22] S. R. White, R. M. Noack and D. J. Scalapino, Phys. Rev. Lett. **73**, 886 (1994).

[23] D. G. Shelton, A. A. Nersesyan and A. M. Tsvelik, Phys. Rev. B **53**, 8521 (1996).

[24] S. Sachdev, *Quantum Phase Transitions*, Cambridge University Press, (2000).

[25] B. K. Chakrabarti, A. Dutta, and P. Sen, *Quantum Ising Phases and Transitions in Transverse Ising Models* Spriger Press (1996)

[26] L. D. Landau and E. M. Lifshitz, *Statistical Physics Part 1.* Course of Theoretical Physics **Vol 5** (3rd ed.), Butterworth-Heinemann, (1980).

[27] P. M. Chaikin and T. C. Lubensky, *Principles of Condensed Matter Physics*, Cambridge University Press, (1995) pp. 214.

[28] E. Stanley, *Introduction to Phase Transitions and Critical Phenomena*, Oxford University Press, (1987).

[29] E. Fradkin, and L. Susskind, Phy. Rev. D **17**, 2637 (1978)

[30] M. den Nijs and K. Rommelse, Phys. Rev. B **40**, 4709 (1989).

[31] M.Oshikawa, J. Phys. Condens. Matter **4**, 7469 (1992)

[32] T. Kennedy and H. Tasaki, Phys. Rev. B **45**, 304 (1992).

[33] Y. Nishiyama, N. Hatano and M. Suzuki, J. Phys. Soc. Jpn. **64**, 1967 (1995).

[34] E. H. Kim, G. Fáth, J. Sólyom and D. J. Scalapino, Phys. Rev B **62**, 14965 (2000)

[35] E. H. Kim, O. Legeza, and J. Sólyom, Phys. Rev B **77**, 205121 (2008)

[36] S. J. Gibson, R. Meyer, and G. Y. Chitov, Phys. Rev.B **83**, 104423 (2011)

[37] G. E. Volovik, *The Universe in a Helium Droplet*, Clarendon Press, Oxford (2003)

[38] J. Cayssol, arXiv: 1310.0792, (2013).

[39] N. Wu, Phys. Lett. A **376**, 3530 (2012)

[40] M. Ezawa, Y. Tanaka, and N. Nagaosa, *Scientific Reports*, **3**, 2790 (2013)

[41] F. Ye and B. W. Xu, Commun. Theor. Phys. (China) **39**, 487 (2003).

[42] J. R. Schrieffer, *Theory of Superconductivity* (W. A. Benjamin, New York, 1964)

[43] E. Barouch, and B. M. McCoy, Phys. Rev. A **3**, 786 (1971)

[44] M.A.Martin-Delgado, R. Shankar, and G. Sierra, Phys. Rev. Lett.**77**, 3443 (1996)

[45] G. Chitov, B. Ramakko, and M. Azzouz, Phys. Rev. B **77**, 224433 (2008).

[46] Xi Dai, and Zhao- bin Su, Phys. Rev. B **57**, 964 (1998)

[47] E. H. Lieb, Phys. Rev. Lett, **73**, 2158 (1994)

[48] I. Affleck, and J.Brad Marston, Phys.Rev. B **37**, 3774 (1988)

[49] M. Azzouz, L. Chen, and S. Moukouri, Phys. Rev. B **50**, 6233 (1994)

[50] G. Gomez-Santos, Phys. Rev. Lett. **63**, 790 (1989)

[51] C Delgi Esposti Boschi, M Di Dio, G Morandi, and M Roncaglia, J. Phys. A: Math. Theor. **42**, 055002 (2009)

[52] M. Azzouz, Phys. Rev. B **48**, 6136 (1993)

[53] M. Azzouz, Phys. Rev. B **74**, 174422 (2006)

[54] G. Y. Chitov, and T. Pandey, arXiv: 1401.xxxx (2014)

[55] K. Okamoto, Phys. Rev. B **67**, 212408 (2003).

[56] M.A. Martin-Delgado, J. Dukelsky, and G. Sierra, Phys. Lett. A **250**, 430 (1998).

[57] V.N. Kotov, J. Oitmaa, and Z. Weihong, Phys. Rev. B **59**, 11377 (1999).

[58] D.C. Cabra and M.D. Grynberg, Phys. Rev. Lett. **82**, 1768 (1999).

[59] Y.-J. Wang and A.A. Nersesyan, Nucl. Phys. B **583** [FS], 671 (2000).

[60] J. Almeida, M.A. Martin-Delgado, and G. Sierra, Phys. Rev. B **76** 184428 (2007)

[61] A. A. Nersesyan, and A. Luther, Phy. Rev. B **50**, 309 (1994)

[62] P. Pfeuty, Ann. Phys, **57**, 79 (1970)

[63] K. Hida, Phys. Rev. B **45**, 2207 (1992)

[64] B. M. McCoy, Phys. Rev. **173** 531 (1968)

[65] G. Fath, O. Legeza, and J. Solyom, Phys. Rev. B **63**, 134403 (2001)

[66] F. Ye, G. H. Ding, and B. W. Xu, Commun. Theor. Phys. (China) **37**, 492 (2002).

[67] E. Lieb, T. Schultz, and D. Mattis, Ann. Phys. (N. y) **16**, 406 (1961)

[68] X. Y. Feng, G. M. Zhang, and T. Xiang, Phy. Rev. Lett. **98**, 087204 (2007)